LBL-24650
c.2

RECEIVED
LAWRENCE
BERKELEY LABORATORY
APR 1 9 1988
LIBRARY AND
DOCUMENTS SECTION

Center for Advanced Materials

CAM

Investigation of Crucible Materials in Gradient Freeze Gallium Arsenide Crystal Growth

J.L. Hurd
(M.S. Thesis)

December 1987

TWO-WEEK LOAN COPY

This is a Library Circulating Copy which may be borrowed for two weeks.

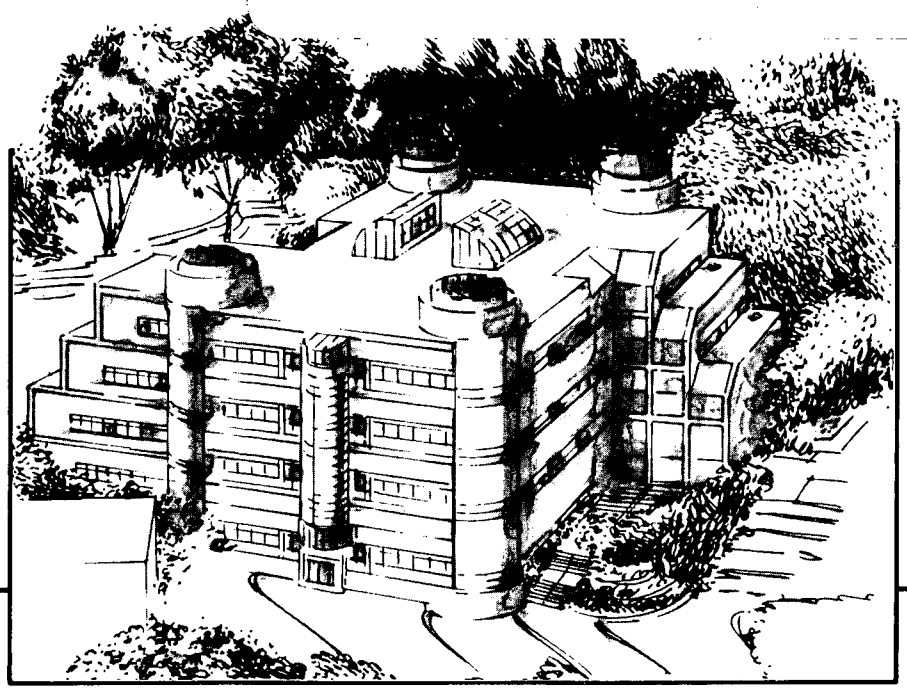

Materials and Chemical Sciences Division

Lawrence Berkeley Laboratory • University of California

ONE CYCLOTRON ROAD, BERKELEY, CA 94720 • (415) 486-4755

Prepared for the U.S. Department of Energy under Contract DE-AC03-76SF00098

LBL-24650
c.2

DISCLAIMER

This document was prepared as an account of work sponsored by the United States Government. While this document is believed to contain correct information, neither the United States Government nor any agency thereof, nor the Regents of the University of California, nor any of their employees, makes any warranty, express or implied, or assumes any legal responsibility for the accuracy, completeness, or usefulness of any information, apparatus, product, or process disclosed, or represents that its use would not infringe privately owned rights. Reference herein to any specific commercial product, process, or service by its trade name, trademark, manufacturer, or otherwise, does not necessarily constitute or imply its endorsement, recommendation, or favoring by the United States Government or any agency thereof, or the Regents of the University of California. The views and opinions of authors expressed herein do not necessarily state or reflect those of the United States Government or any agency thereof or the Regents of the University of California.

LBL-24650

Investigation of Crucible Materials in Gradient Freeze Gallium Arsenide Crystal Growth

Jeffery L. Hurd

M.S. Thesis

Department of Materials Science and Mineral Engineering
University of California, Berkeley

and
Center for Advanced Materials
Lawrence Berkeley Laboratory
Berkeley, California 94720

December 1987

This work was supported by the Director, Office of Energy Research, Office of Basic Energy Sciences, Materials Science Division of the U. S. Department of Energy under contract DE-AC03-76SF00098.

ABSTRACT

Undoped synthesized GaAs and crystals grown by the gradient freeze method were analyzed by room temperature Hall effect for net carrier concentration, secondary ion mass spectroscopy for silicon and residual impurity concentrations, localized vibrational mode spectroscopy for carbon concentration, and optical absorption for neutral EL2 concentration. Impurity compensation was examined to determine limits for silicon concentration in semi-insulating GaAs. Boules synthesized in a variety of materials are used to determine the residual impurity concentrations contributing to compensation. Shallow donor concentrations below the residual acceptor concentration resulted in semi-insulating electronic properties for two synthesis boules. The silicon incorporation rate in gradient freeze crystals is quantified through the deviation of net donor concentration from the normal freeze distribution. Crystals grown As rich, Ga rich and near stoichiometric composition in SiO_2 crucibles show order-of-magnitude differences of silicon incorporation rate. Crystals grown in Al_2O_3 and graphite crucibles have less than 10^{-2} and greater than 3 times respectively the incorporation rates of gradient freeze GaAs grown in SiO_2 crucibles. Crystals grown in a vertical gradient freeze configuration have less than 1/7 the incorporation rate of those grown horizontally. A vapor mechanism for incorporation of silicon is indicated, irrespective of crucible material, that contributes enough silicon to preclude semi-insulating properties. At high values of net donor concentration, an acceptor concentration is seen that may be of native defect origin and is positively correlated with net donor concentration.

ACKNOWLEDGMENTS

I would like to thank my advisor, Professor Eugene Haller for his support and encouragement throughout this work. Dr. Edith Bourret and Joseph Guitron are gratefully acknowledged for their helpful discussions, ongoing interest in this work and for the GaAs crystal growth.

I would like to express my appreciation to Dr. Robert McMurray, In-Shik Park, and Wai Fan Yau who contributed to some of the optical and I.R. measurements in this work, Dr. Kin Man Yu, who provided Rutherford backscattering data, and X-ray diffractometer spectra for BN films, and David Bliss for many useful discussions. I would like to thank Dick Davis and Jeff Beeman for their technical advice and assistance.

I would also like to express my appreciation to Dr. W. Walukiewicz and Dr. Dale Perry for their interest in this work, and to Professor Eicke Weber and Professor Dennis Hess for reading and commenting on the manuscript.

The advice and encouragement of Richard Axton, Dr. V. Ramanathan, and Professor Sigurd Wagner is gratefully acknowledged. Finally I wish to thank my family and friends for their support and Dr. P. Tejedor whose encouragement and support made this possible.

This work was supported by the Director, Office of Energy Research, Office of Basic Energy Sciences, Materials Science Division of the U. S. Department of Energy under contract DE-AC03-76F00098.

Table of Contents

Page

1.0 Introduction

1.1 Interest in gallium arsenide bulk crystals..... 1

1.2 Impurities and defects in GaAs

1.2.1 Isovalent and electrically active impurities..... 3

1.2.2 Segregation and impurity incorporation..... 4

1.2.3 Intrinsic defects..... 5

1.2.4 Semi-insulating GaAs..... 9

1.3 Growth techniques for semi-insulating GaAs

1.3.1 Liquid Encapsulated Czochralski growth..... 11

1.3.2 Horizontal gradient freeze growth..... 13

1.3.3 Vertical gradient freeze growth..... 16

1.4 Aim and objectives..... 18

2.0 Experimental procedures and results

2.1 Synthesis and gradient freeze crystal growth

2.1.1 Standard growth process

2.1.1.1 Synthesis and growth..... 19

2.1.1.2 Starting material impurities..... 21

2.1.2 Crucible materials and impurities in synthesis

2.1.2.1 Preliminary synthesis with crucible liners..... 23

2.1.2.2 Boron nitride film on silica crucibles..... 25

2.1.2.3 Synthesis impurities and arsenic pressure effects..... 27

Page

2.1.3 Silicon incorporation during growth..... 33

2.1.3.1 Incorporation rate measurement..... 33

2.1.3.2 Baseline incorporation - silica cloth-lined crucible..... 37

2.1.3.3 Arsenic pressure effects in silica cloth-lined crucibles..... 37

2.1.3.4 Aluminum oxide cloth lined crucible..... 39

2.1.3.5 Graphite crucible..... 42

2.1.3.6 Silicon incorporation in vertical gradient freeze growth..... 45

2.1.3.7 Silicon incorporation rates - summary..... 47

2.2 Arsenic permeability experiments

2.2.1 Graphite permeability..... 47

2.2.2 Synthesis in a sealed graphite container..... 49

3.0 Discussion

3.1 Effects of crucible materials in synthesis..... 51

3.2 Effects of crucible materials in growth..... 58

3.2.1 Graphite crucible..... 58

3.2.2 Silica crucibles..... 62

3.2.3 Alumina crucible..... 66

3.3 Silicon incorporation during vertical growth..... 67

4.0 Summary and conclusions..... 68

Page

5.0 Appendix

5.1 Procedure for making ohmic contacts on bulk GaAs for Hall effect..... 72

5.2 Effect of grain boundary on carrier concentration and mobility..... 73

6.0 References..... 75

1.0 Introduction

1.1 Interest in gallium arsenide bulk crystals

Gallium arsenide (GaAs) is rapidly becoming a major material in the microelectronics industry (1). It is a direct band gap material (~1.43eV) of relatively high electron mobility (8600 $cm^2/Vsec$) compared to silicon (1350 $cm^2/Vsec$) at 300 K (2). The direct bandgap allows for the efficient direct recombination of electrons and holes, resulting in light emission. This basic property has been extensively used in light emitting diodes and solid state lasers. More recently, the high electron mobility has been utilized in fast switching integrated circuits (IC's). The maximum electron drift velocity is $2x10^7$ cm/sec at the low electric field of 3.5 kV/cm at room temperature (3). Intrinsic gallium arsenide has not been produced so far because of the low intrinsic carrier concentration ($n_i \simeq 9x10^6 cm^{-3}$) (2). No material intrinsically has the high degree of purity required to attain this carrier concentration and compensation with shallow dopants to attain it could only be maintained over extremely small regions of a crystal. There is, however, a serendipitous attribute of GaAs that permits the growth of large crystals which exhibit intrinsic behavior. The existence of a predominant native mid-gap donor level makes it possible to maintain the Fermi level close to midgap if the net shallow acceptor concentration is smaller than the concentration of the midgap level. This creates a condition similar to intrinsic behavior. Recombination

of carriers to this level brings the net carrier concentration close to the intrinsic level. The material is now an insulator that may be doped in selected locations or patterns by ion implantation, alloying or diffusion. The semi-insulating (SI) material is used as a highly insulating substrate for devices in large scale integrated circuits. The high resistivity of the substrate provides for device isolation over small dimensions facilitating a high device density. Coupled with the high switching speed, and optical interfacing between a circuit and the outside wiring, the material has a number of distinct advantages over silicon for integrated circuits.

Being still a relatively new material for integrated circuits, GaAs poses a number of problems which have to be solved. The threshold voltage for turning a field effect transistor (FET) (the smallest functional unit of an IC) on or off may be influenced by dislocations and associated high local impurity concentration within their vicinity. Dislocations can affect the FET threshold voltage (1). Dislocation density must be low for good device reliability. This may become more of a problem as the device density approaches the dislocation density (4). The devices in the regions of high dislocation density would be expected to fail first. After ion implantation, an annealing step at temperatures above 800°C for ~30 min is required to activate the implanted layer and to remove damage introduced by the implantation (5). The concentration of the mid-gap level can be affected during annealing, but it must always exceed the net shallow acceptor concentration for semi-insulating conductivity.

Several considerations are important in the growth of GaAs bulk

crystals for use in IC's. The dislocation density and uniformity, the shallow donor and acceptor compensation, the concentration and uniformity of deep level defects, the thermal stability of the SI properties of the as-grown material, and the crystal shape are the most critical parameters in that they all affect the subsequent performance and yield of devices. These properties can all be affected by the particular growth technique employed due to the wide range of conditions to which the growing crystal can be subjected. By using appropriate materials in contact with the melt during growth and a suitable growth process, GaAs can be grown with SI properties.

1.2 Impurities and defects in GaAs

1.2.1 Isovalent and electrically active impurities

To a first approximation, the number and types of ionization states for a substitutional impurity are determined by the number of s and p orbital valence electrons the impurity has relative to the number used by covalent bonding in the lattice. Shallow donors and acceptors can be grouped according to position in the periodic table. Gallium is a group III element, arsenic is a group V element. Group II elements will be acceptors on a Ga site. Group III elements will occupy the gallium site isovalent with gallium and will not produce an electronic effect. Group IV elements are observed to occupy either the Ga or As site, being either donors or acceptors respectively. Carbon has not been seen to occupy the gallium site, perhaps due to its small atomic radius relative to gallium. Si is amphoteric,

although it is preferential to the gallium site in bulk single crystals. Group V elements are isovalent with and tend to occupy arsenic sites. Group VI elements are donors on arsenic sites. The transition metals have energy levels within the gap depending on the specific impurity's tendency to donate or accept electrons. The energy level and ionization state for a given impurity atom may not be predictable due to the tendency to form impurity-defect complexes (3,6) at high concentrations. The position of the Fermi level will determine the solubility and consequently the distribution on donor or acceptor sites for an amphoteric dopant (7,8). A deviation from stoichiometry may also affect this distribution. The degree to which the distribution is affected by stoichiometry is not known for GaAs. A discussion of some impurities in GaAs and their relative energy levels is presented in section 2.1.1.2.

1.2.2 Segregation and impurity incorporation

The fraction of impurities that incorporate in the solid relative to those in the liquid is called the segregation coefficient. It is found from the equilibrium diagram gap between the liquidus and solidus for a particular concentration of impurity. At low concentrations, this value will be a constant:

$$K_{eq} = \frac{C_{solid}}{C_{liquid}} \qquad (1.1).$$

More commonly, an effective segregation coefficient somewhat closer to unity than the equilibrium coefficient is used due to non-complete mixing of the liquid phase and accumulation of impurities

at the growing interface. For a normal freeze growth process with complete mixing of the melt and no solid diffusion, the impurity concentration in the solid, C_s, is related to the fraction solidified by (9):

$$C_s = k\ C_o\ (1-g)^{k-1} \tag{1.2}$$

where g = fraction solidified, k = effective segregation coefficient, and C_o = initial solute concentration in the melt. When impurities are added during the growth process (e.g. when some crucible material is dissolved by the melt), this equation must be modified as shown in section 2.1.3.1.

1.2.3 Intrinsic defects

Defect equilibrium in a binary compound is complex due to the large number of defect types and their mutual interactions. For charged defects, the situation is further complicated by the concentration of electrons and holes (or position of the Fermi level) affecting the charge states of the point defects. Several point defects can be assumed to exist in some concentration in a crystal. The stoichiometry of the compound is a primary factor in determining the types of defects that can be presumed to predominate. Here "o" denotes neutral, "+" a positive, and " - " a negative effective charge relative to the lattice. A positive (negative) charge indicates the defect is an ionized donor (acceptor). The electronic levels for these defects can lie anywhere inside or outside the band gap of GaAs, but they usually have a larger ionization energy than purely hydrogenic shallow donors and acceptors. Typically they are deep levels with a strong, localized potential near the origin of the defect.

Calculations using a self-consistent Green's function technique (10) indicate that for Ga-rich crystals, we would expect arsenic vacancies V_{As}^{+} and gallium interstitials Ga_{i}^{+} will be favored. Gallium atoms on the arsenic sublattice, Ga_{As}^{-2}, otherwise called gallium antisite defects may also predominate.

In arsenic rich GaAs, gallium vacancies V_{Ga}^{-2}, V_{Ga}^{-3}, arsenic interstitials As_{i}^{o}, As_{i}^{+}, As_{i}^{+2}, As_{i}^{+3}, and arsenic antisite defects As_{Ga}^{o}, As_{Ga}^{+}, and As_{Ga}^{+2} will be favored.

All native defects undergo mass action law type reactions while cooling after solidification. These can be expressed generally following Baraff and Schlüter (10) :

$$N_A A + N_B B = N_C C + N_D D \qquad (1.3)$$

where A, B, C, and D are defect types and N_A, N_B, N_C, and N_D are the numbers of defects present in the equation. Each reaction has an associated equilibrium constant:

$$K = \frac{[C]^{N_C} \times [D]^{N_D}}{[A]^{N_A} \times [B]^{N_B}} = e^{-\Delta G/kT} \qquad (1.4)$$

where ΔG is the change in Gibbs free energy for the reaction. A

further constraint is the deviation from stoichiometry:

$$\delta = \frac{N_{As} - N_{Ga}}{N_{As} + N_{Ga}} = M_A[A] + M_B[B] + \ldots\ldots \qquad (1.5)$$

where M_n is a sum of +1 (-1) for every extra (missing) arsenic atom and -1 (+1) for every extra (missing) gallium atom the defect contributes to the lattice (e.g. +2 for As_{Ga}, +1 for Si_{Ga}). Free electrons and holes are considered defects in this definition but would have no effect on δ. The position of the Fermi level will determine the charge state of each individual defect. The concentration of each defect is a function of temperature and arsenic pressure during growth or annealing. Defects will be frozen into the lattice as the crystal cools and the concentration of each defect will be a function of its environment and its cooling history. The full solution for the mass action law equations is not known due to lack of experimental data for equilibrium constants of defect reactions. Defects of opposite charge tend to form pairs and impurities often combine with defects forming impurity-defect complexes, which further complicates the analysis.

The assignment of defects to the various levels requires correlation between at least 28 electronic levels (11) and their defect nature (12). Considerable work is being carried out, but definitive progress is slow. Controversy still reigns after over 20 years investigation of the midgap level or levels responsible for the semi-insulating nature of GaAs. It is generally accepted, however,

that this is the EL2 level and that it is related to the arsenic antisite As_{Ga} and another defect such as an As_i (13) or a V_{As} (14).

To analyze the energy and concentration of deep levels arising due to defect states, the deep level transient spectroscopy technique (DLTS) is most useful (15). Parsey (16) investigated seven major states in horizontal Bridgman material, three present at concentrations greater than 10^{16} cm^{-3}: EL2, EL5, and EL6. The thermal activation energies measured for these donors were E_c-.75 eV, E_c-.4 eV, and E_c-.34 eV respectively. The deep state EL2 was found to increase by a factor of 5 as the arsenic source temperature (and therefore the arsenic fraction in the solid, X_{As}) was increased from 613 to 628°C. The concentration of EL2 varied from $9x10^{15}$ to $5x10^{16}$ cm^{-3}. The maximum concentration of EL5 was $1.5x10^{16}$ cm^{-3}, and EL6 was $3x10^{16}$ cm^{-3}, but these levels did not correlate with X_{As}. All three levels were found to be suppressed by a high net donor concentration. The suppression followed an n^{-4} dependency with EL2 and EL5 concentrations; an n^{-3} dependency with EL6 concentration.

The concentration of neutral $EL2^o$ may be measured through optical absorption in the near IR (1.1μm) (17,18). Such measurements have been correlated to DLTS data to give quantitative results.

Parsey (16,19) further found a strong correlation of dislocation density with arsenic vapor pressure. He determined the optimum arsenic source temperature to be 617°C to minimize the dislocation density to less than 500 cm^{-2} in undoped crystals using the horizontal Bridgman method. This temperature is also considered to be very close to the

temperature for growth of stoichiometric GaAs. The temperature for exact stoichiometry is not known, however, since dislocations are primarily dependent on vacancy concentrations and the presence of other defects would shift this temperature from the point of minimum dislocation density. For a 3°C deviation above and below 617°C, dislocations were found to increase to approximately 10^4 cm^{-2}.

1.2.4 Semi-insulating GaAs

For GaAs to become semi-insulating, it is necessary that the compensation be such as to allow only mid-gap levels to contribute free carriers to the conduction band at low (typically 10^7 - $10^8 cm^{-3}$) concentrations due to their high ionization energy. In a simplified three level model the levels considered are: shallow donors with concentration N_D, shallow acceptors with concentration N_A, and deep level mid-gap donors with concentration N_{DD} (20,21). The necessary conditions for SI behavior to occur are: 1) The concentration of acceptors N_A must be greater than the concentration of shallow donors N_D, and 2) the number of mid-gap donors must be greater than N_A-N_D, the remaining acceptors not compensated by shallow donors. Without a mid-gap level present, this would be p-type material. Figure 1 illustrates this compensation model. The situation can become more complex if, e.g., chromium acceptors are added as is done for heavily Si-doped n-type material to produce SI material. This procedure is not advantageous due to the reduction of majority carrier mobility accompanied by the increase of ionized impurity scattering. Also, chromium has been shown to be a rapidly diffusing impurity. For the gradient freeze crystals used in this study, N_D is primarily the net

$[Si_{Ga}]-[Si_{As}]$ donor concentration, N_{DD} is the EL2 concentration, and N_A is the residual acceptor concentration. For these crystals, a three level model suffices.

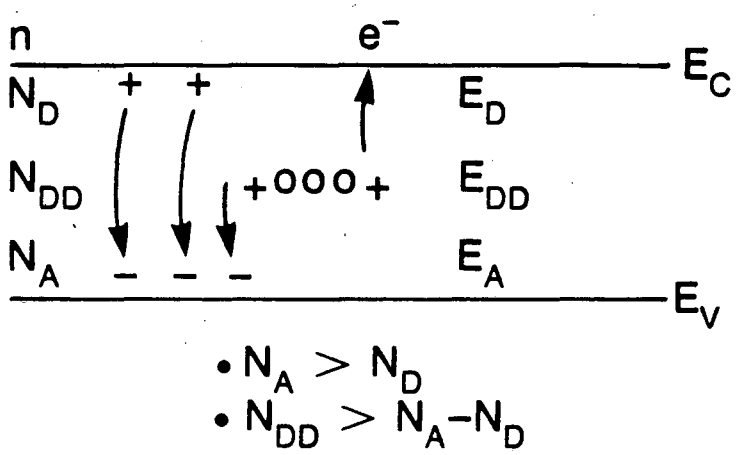

XBL 8711-5987

Figure 1 Three level compensation model for semi-insulating GaAs.

1.3 Growth techniques for semi-insulating GaAs

1.3.1 Liquid Encapsulated Czochralski growth

Typically, GaAs is grown by the Liquid Encapsulated Czochralski (LEC) technique. The melt is surrounded by a liquid B_2O_3 encapsulant to avoid the evaporative loss of arsenic. A high or low inert gas ambient pressure is used. In high pressure growth, the GaAs is synthesized in situ from the elements in a pyrolytic boron nitride (PBN) crucible under a B_2O_3 melt encapsulant reacting exothermally beginning at ~820°C under a pressure of 60 atm (22). The reaction continues until the 1238°C melting point of GaAs is reached. The pressurized encapsulant reduces arsenic evaporation, but control of stoichiometry is difficult due to some uncontrolled loss of arsenic and uncertainties in the initial charge composition. Low pressure growth uses less than 5 atm gas pressure and employs an externally heated arsenic source to achieve stoichiometry prior to growth. This does not prevent arsenic loss during growth, however. Growth is initiated by lowering a rotating seed crystal through the encapsulant, contacting the melt to pull a nominally cylindrical crystal of varying diameter. The typical growth rate is ~8mm/hr. A high thermal gradient (100-150°C/cm) and non-planar interface generate high thermal stresses upon cooling which result in dislocation densities typically greater than $10^4 cm^{-2}$. The dislocation density typically follows a characteristic W-shaped concentration profile across wafers cut from the crystals. The concentration of EL2 follows a similar pattern and is often correlated with dislocation density (23,24). The EL2

concentration is more homogeneous after annealing at 950°C for 100-200 hours (25). Both the thermally induced stress and high dislocation density can be reduced by the addition of an annular crucible lid that reduces the radial thermal gradient. Dislocation densities were reported of less than $1000cm^{-2}$ in the central portion of wafers cut from crystals grown in this configuration (26). Indium doping (27) and the use of a thermal baffle and increased heating of the B_2O_3 layer (28,29), acting to reduce the thermal gradient during cooling, all have been effective to some degree in reducing dislocation densities.

The use of a PBN crucible for LEC growth of GaAs (30) results in low concentrations of silicon: $[Si] < 2x10^{15}cm^{-3}$. Carbon is present as the primary acceptor impurity ($[C] \approx 3\text{-}15\ x10^{16}cm^{-3}$) that compensates the silicon donors. The presence of carbon is most likely due to carbon furnace parts introducing CO and CO_2 into the growth environment. When the As fraction is increased above a critical value ($X_{As} \approx 0.475$), the EL2 concentration increases to a point where the conduction behavior changes from p-type to semi-insulating.

More recent work (31) reports significantly less carbon and silicon impurities: $[C] = 3x10^{14}cm^{-3}$, and [Si] less than $2x10^{14}cm^{-3}$. The total impurity donor and acceptor concentration were each less than $2x10^{15}cm^{-3}$. The total donor and acceptor concentration, however, were each in the mid $10^{15}cm^{-3}$ range indicating significant native defect concentrations. The EL2 concentration was increased by annealing, from the as grown concentration of $6x10^{15}cm^{-3}$ to $1.0x10^{16}cm^{-3}$. The resistivity could be modulated between SI and conductive by varying the cooling

rate after a 950°C anneal, indicating a defect controlled compensation.

1.3.2 Horizontal gradient freeze growth

Horizontal Bridgman growth techniques (16,19,32) commonly use a moving furnace and a stationary quartz boat within a sealed quartz ampule. The horizontal gradient freeze (HGF) method used for this work is similar, but all parts are stationary and the furnace temperature profile is varied electronically. The crystal and melt are subjected to a temperature gradient through the independent control of a number of closely spaced heater elements, linked with thermocouples situated along the growth axis. Stoichiometry is maintained by very careful thermal control of the arsenic pressure in the ampule, but remote from the melt. The temperature of this source is held very near an optimum value of 617°C to provide the correct vapor pressure for minimum dislocation density. The furnace is normally tilted from horizontal to compensate for the thermal expansion of GaAs upon freezing, which would otherwise produce a constantly increasing crystal cross sectional area. Figure 2 illustrates the HGF configuration.

A significant difficulty inherent to these techniques is the asymmetrical thermal configuration. As can be seen in figure 2, the boat is situated in the lower half of the ampule. The solid angle of radiative surface seen by the various parts of the crystal does not produce equivalent radiative heating to both the top and bottom of the crucible. Also, convection in the melt affects the thermal symmetry at the growth interface. The primary result of this thermal asymmetry is a solid-liquid interface that is concave to the growth direction. In addition, the axial temperature gradient drives a convective current

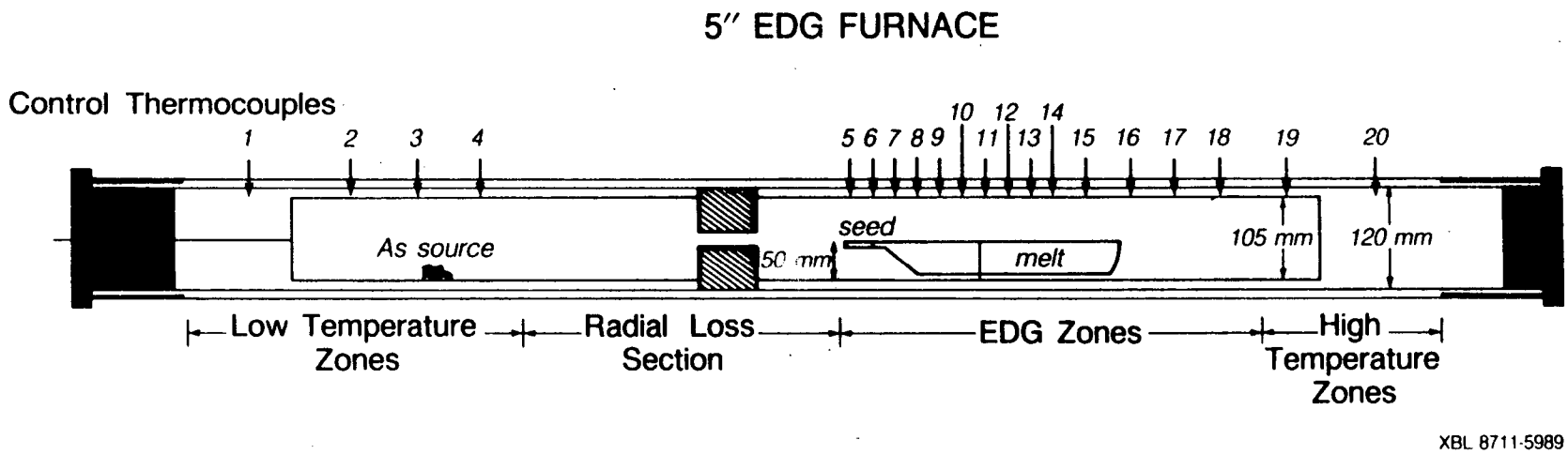

Figure 2 Electro-dynamic growth furnace for growth of GaAs by the horizontal gradient freeze method.

that promotes the interface curvature. The solid-liquid interface shape has been correlated to the propagation of defects in directional solidification (33). For a planar interface, thermal stress and hence dislocation density are generally minimized. The gradient freeze method employs a low thermal gradient (~10°C/cm) during growth. The thermal stresses produced by this method are much less than for LEC growth, resulting in a low (~500cm^{-2}) defect density. Due to the horizontal boat crucible configuration, crystals have a "D"-shaped cross section, a problem for large scale processing where a circular geometry is preferred. Growth in boats with only a small slot near the top for exposure to arsenic vapor would decrease the cross section problem, but would not decrease thermally driven convection in the melt.

Fused silica (SiO_2) is commonly used for the crucible material in HGF growth of GaAs. The surface of the crucible is sandblasted to produce roughness which minimizes wetting and eliminate subsequent sticking of the solid GaAs to the crucible (32). This eliminates stress produced from the differential expansion of the GaAs and the crucible upon cooling. Also through surface tension the liquid rides on the sharp peaks of the surface, decreasing the surface area exposed to the melt. This reduces the chance for nucleation of grains or for twinning.

The SiO_2 crucible is the primary source of Si impurity. The ampule enclosing the SiO_2 boat, GaAs, and As source is also made from SiO_2. It is possible that some degree of silicon doping of the melt can occur through exposure of the ampule walls to As vapor and subsequent vapor transport to the melt.

Silicon is incorporated through the dissolution of the crucible by the reaction (34):

$$4Ga(l) + SiO_2(s) = Si(sol) + 2Ga_2O(v) \qquad (1.6)$$

where (sol) indicates "in solution". For the reaction to proceed, the Ga_2O vapor must be removed to a colder portion of the ampule to condense by the reaction:

$$3Ga_2O(v) + As_4(v) = Ga_2O_3(s) + 4GaAs(s) \qquad (1.7).$$

Considering the concentration of silicon required to produce n-type material, [Si] ≈ 1 ppm , and a typical growth rate of ~4 mm/hr, the reactions need not proceed rapidly to affect the silicon doping concentration.

A recent attempt to reduce this reaction rate employed a 1-2 mm x 140 mm capillary tube as a diffusion barrier between the cold and hot sections of an ampule in the analogous growth of InP by a solute diffusion technique (35). Si contamination was reduced by approximately a factor of 10.

1.3.3 Vertical gradient freeze growth

A possible improvement to the GF method is through modification to a vertical configuration. A number of advantages are created (36): 1) the thermal environment of the crystal and melt is now radially symmetric, allowing the possibility of a planar or convex growth interface, thereby reducing the concentration of strain-generated

dislocations, twin and grain propagation, 2) convection of the melt is reduced, decreasing impurity striations and inclusions in the crystal, and 3) the crystal has a circular cross section and exact diameter control. The vertical gradient freeze (VGF) technique has been demonstrated for the growth of strain and striation free GaP (37) from a PBN crucible. A reduction of dislocation density to $10^3 cm^{-2}$ was seen which is one to three orders of magnitude below the LEC values for this material. In an attempt to scale up this process, another investigation (38) concluded that single crystal growth was difficult due to "spurious nucleation at the crucible-melt-seed line". More recently, 50mm diameter single crystals of GaAs, GaP, and InP were grown by VGF (39). Si doped and undoped GaAs crystals were grown in PBN crucibles. The silicon doped crystals had very low dislocation densities ($\sim 300 cm^{-2}$). The undoped GaAs was semi-insulating and was resistant to thermal conversion (to p-type) during annealing at 800°C for 30 min.

PBN is currently widely used in LEC growth of low-silicon content SI-GaAs crystals. Its use in gradient freeze growth has not been fully explored. Due to the high cost of PBN crucibles (40), it is advantageous to develop alternatives such as coatings or liners of BN and other materials inside less expensive silica and graphite crucibles.

1.4 Aim and objectives

Silicon impurity incorporation from the growth environment is the most significant limitation to the gradient freeze growth of SI GaAs. The aim of this work is to:

1) determine the maximum silicon concentration allowable in semi-insulating GaAs based on the residual impurities present in the starting materials;

2) establish a method to quantify the extent of silicon impurity incorporation during growth;

3) establish the magnitude of suppression of incorporated silicon carriers due to stoichiometry variations;

4) explore several possible crucible materials, the extent these materials incorporate into the crystal, and the associated electronic effects;

5) select and use new crucible materials, coatings and liners for horizontal and vertical gradient freeze growth of device-quality SI-GaAs.

2.0 Experimental procedures and results

2.1 Synthesis and gradient freeze growth

2.1.1 Standard growth process

2.1.1.1 Synthesis and growth

The horizontal gradient freeze technique was described in section 1.3.2. The GaAs bulk crystals used in this work were grown in a five inch I.D. Mellen "Electro Dynamic Gradient" (EDG) furnace (41). Figure 2 shows the EDG multi-zone furnace system. The low temperature zone contains the arsenic source at a controlled temperature. At 617°C the As vapor pressure is in equilibrium with the partial vapor pressure of As (~1 atm.) over stoichiometric gallium arsenide at its 1238°C melting point. It has been shown by Parsey (16,19) that a minimum in dislocation density is obtained for small crystals grown with a 617°C As source temperature. A temperature lower than 617°C will produce a gallium-rich crystal, a higher temperature will result in an arsenic-rich crystal. The radial loss section is used to isolate the low and high temperature sections. The boat, seed and growing crystal, and melt are contained in the EDG furnace section.

Crystals grown using two processes were analysed: 1) separate synthesis and growth, and 2) in-situ synthesis and growth. Both processes will be described for SiO_2 crucibles and liners, but the processes will be the same for the investigation of other crucible materials in section 2.1.3. Section 2.1.2 considers only synthesis in the investigation of crucible materials.

Synthesis is accomplished using SiO_2 crucibles that are sandblasted with number 80 grit SiC, cleaned to remove all SiC particles, and etched in aqua regia (HCl/HNO_3,3:1). The crucible containing elemental Ga is placed in the ampule remote from the As. The ampule is then evacuated, backfilled with N_2 and evacuated again to less than $3x10^{-5}$ torr before being sealed. The temperatures of both the arsenic source and crucible are increased simultaneously, both to follow the temperatures at which the arsenic vapor pressure is in equilibrium with the Ga-As phases present in the crucible (i.e., the gallium liquid saturated with arsenic, and the solid GaAs). The final state after heating for 3.5 hours is 617°C As temperature in near equilibrium with GaAs liquid at 1242°C (just above its 1238°C melting point). These temperatures are maintained for 2 hours to allow the liquid GaAs composition to reach equilibrium. The system is then cooled at 60°C/hr.

For growth, synthesized GaAs is then placed in an SiO_2 crucible, lined with a coarse woven SiO_2 fabric (to avoid wetting) and containing a seed crystal at one end. A similar 3.5 hour heat-up as in synthesis is then carried out, before melt-back of the seed. A thermal gradient of 4 to 10°C is applied axially to the crystal length, and the overall temperature is decreased to initiate growth from the seed. A growth rate of 4mm/hr is used and the crystal length is typically 300 mm. After growth, the crystal is cooled at 60°C/hr.

The in-situ synthesis and growth process is practically identical to a combination of the separate synthesis and growth steps; but the transfer of the GaAs prior to growth and any associated impurity

contamination is avoided.

2.1.1.2 Starting material impurities

To determine the sources of impurity in the crystals, it is necessary to know the concentrations of impurities present in all of the materials used during growth. The material used to make the ampule, the gallium and arsenic, and the materials used for crucibles and crucible liners all contain trace impurities. The electrically active impurities in silica (GE 214), are below 10 ppm so that the SiO_2 itself is the main source of contamination. The impurity concentrations of the silica cloth (Astroquartz II, J.P. Stevens) are not known precisely, however they are believed to be higher than in bulk SiO_2. All impurities measured for the gallium (Alusuisse-7N) are below the atomic absorption detection limits.

For impurities other than silicon and oxygen, the elemental arsenic is the primary source of contaminating impurities. An analysis of impurity concentrations determined by emission spectroscopy for 4 batches of arsenic (6N) was obtained from the supplier. The highest concentrations from these values were then converted to concentrations the GaAs would contain if all impurities from the arsenic were incorporated into the crystal. Table 1 lists the resulting maximum concentrations in crystals due to these impurities. Only a limited number of elements are available in this analysis. The highest concentration acceptor is iron. Calcium and silicon are also present in measurable concentrations. The electronic behavior of calcium in GaAs is not known, however it is most likely a shallow acceptor on the gallium site due to its two valence electrons. Based on these data,

the concentration of shallow acceptors in GaAs due to impurities in the arsenic is expected to be below $10^{16}cm^{-3}$. It is also expected that a portion of those impurities which are non-volatile at 617°C remain in the arsenic source section of the ampule. Impurities that do not incorporate from outside sources of contamination will be incorporated according to their respective segregation coefficients. The impurity concentration will be higher toward the tail end of crystals for elements with k<1.

Table 1. Maximum concentrations obtained by emission spectroscopy for selected impurities in four batches of arsenic obtained from one supplier. The maximum possible concentration in the GaAs due to these impurities is tabulated in column 3. Binding energies were obtained from references 3 and 42, segregation coefficients from reference 43.

Element	Maximum concentration in arsenic (ppm)	Maximum concentration in GaAs (cm^{-3})	Expected Doping Behavior	Binding energy (meV)	Segregation coefficient k
Al	<0.28	$<6.2 \times 10^{15}$	neutral	---	n.a.
Ag	<0.007	$<1.5 \times 10^{14}$	acceptor	n.a.	n.a.
Ca	0.19	4.1×10^{15}	n.a.	n.a.	n.a.
Cu	<0.12	$<2.6 \times 10^{15}$	acceptor	23,150,240,510	n.a.
Fe	0.13	2.9×10^{15}	acceptor	370,520	0.001
Mg	<0.31	$<6.9 \times 10^{15}$	acceptor	12,29	n.a.
Pb	<0.036	$<8.0 \times 10^{14}$	donor	5.8	n.a.
Si	0.27	6.0×10^{15}	amphoteric	5.9(d),34.8(a)	0.14

(<) indicates detection limit, (n.a.) not known or available.

2.1.2 Crucible materials and impurities in synthesis

2.1.2.1 Preliminary synthesis with crucible liners

Prior to actual synthesis and growth in new materials, six materials were investigated in trial synthesis experiments. The intent of this was to determine the feasibility of GaAs growth in a number of available materials, and to eliminate those that qualitatively performed poorly in two critical categories: 1) the degree of sticking of the GaAs to the material upon its removal from the crucible, 2) the degree of wetting, measured from the approximate contact angle of the GaAs to the material after solidification. Results from this experiment were used to choose materials for subsequent seeded growth runs.

One inch diameter hemispherical fused silica crucibles with coatings or liners of the materials of table 2 were used for synthesis crucibles. Of particular interest was a BN coating due to the successful implementation of solid pyrolytic BN crucibles in LEC semi-insulating GaAs growth. The coating was a suspension of BN particles in methanol which was sprayed and allowed to dry on the surface of the crucible. In a separate experiment, three graphite crucibles with three degrees of surface roughness were used.

Table 2 gives qualitative ratings in all three categories for the materials tested. In some cases, a discoloration of the liner material indicated that a chemical reaction had occurred. When the liner dissociated or fine particles were present, a slag of floating particles appeared on the surface of the GaAs. Hall effect measurements were made where feasible. In most cases the GaAs was too

Table 2. Relative rating of crucible materials in categories of observed sticking and wetting (0 to 4 increasing) based on trial GaAs synthesis experiments.

Sample Number	Crucible Material	Sticking	Wetting	Description	N_D-N_A ($x10^{16}cm^{-3}$)
1	BN coating	1	1	BN inclusions	370
2	Al_2O_3cloth	0	1		170
3	ZrO_2 knitted	2	2	discoloration	16
4	ZrO_2 woven	3	3	discoloration	6.5
5	ZrB_2 coating	2	1	slag and floating particles	630
6	Y_2O_3coating	4	4	sticks to crucible slag, reactive	---
7	ZrO_2 (Y_2O_3 binder)	2	2	discoloration	---
8	ZrO_2 felt (Y_2O_3 binder)	2	2	discoloration	---
9	Al_2O_3 felt	1	1		---
10	Graphite (polished)	0	2		---
11	Graphite (medium coarse)	0	2	slag and floating particles	---
12	Graphite (coarse)	1	1	slag and floating particles	---

inhomogeneous to obtain meaningful data. Hall measurements of samples 1-5 showed a heavy n-type doping. These samples were synthesized in one ampule and it is possible that cross-contamination occurred. The amount of SiO_2 present in the crucible materials is not known. The Al_2O_3 cloth used for sample 2 was Zircar AlW30A containing less than 1 percent SiO_2. BN inclusions and a high net carrier concentration measured for the GaAs ingot synthesized in the BN coated crucible precluded the subsequent use of this coating technique. BN and Al_2O_3 showed less wetting and sticking compared to other tested

materials. Of these potential crucible materials, Al_2O_3 cloth, graphite, and BN (grown by medium temperature CVD and pyrolytic BN) were subsequently investigated in synthesis or seeded growth.

2.1.2.2 Boron nitride film on silica crucibles

Chemical vapor deposition (CVD) of the low pressure stable hexagonal phase of boron nitride (BN) on SiO_2 substrates has been previously reported (44,45). In addition, a solid pyrolytic boron nitride (PBN) crucible has been used for in-situ synthesis and growth (46). BN films on silica crucibles were used in this work to separate the melt from direct contact to the silica during synthesis with the intent of reducing silicon incorporation.

1 to 20 μm thick BN films were prepared on two sandblasted SiO_2 synthesis boats. The deposition furnace schematic is shown in figure 3. BCl_3 (99.9 percent) and NH_3 (99.998 percent) gases diluted with argon are mixed as they exit two gas manifolds located directly below the inverted crucible. Flow rates of 0.02 l/min BCl_3 and 0.04 l/min NH_3 are diluted with Ar for a total flow rate of 0.25 l/min. The furnace thermal profile is peaked near the center of the crucible at 1100°C. The crucible ends are ~ 50°C cooler. Two flat SiO_2 plates were mounted perpendicular to the gas stream inside a crucible during deposition. The deposition rate is approximately 4μm/hr.

BN films deposited on these plates were characterized by three methods: 1) x-ray diffraction for structure determination, 2) optical absorption for band gap measurement, and 3) Rutherford backscattering for thickness determination.

An X-ray diffractometer spectrum was taken of the substrate

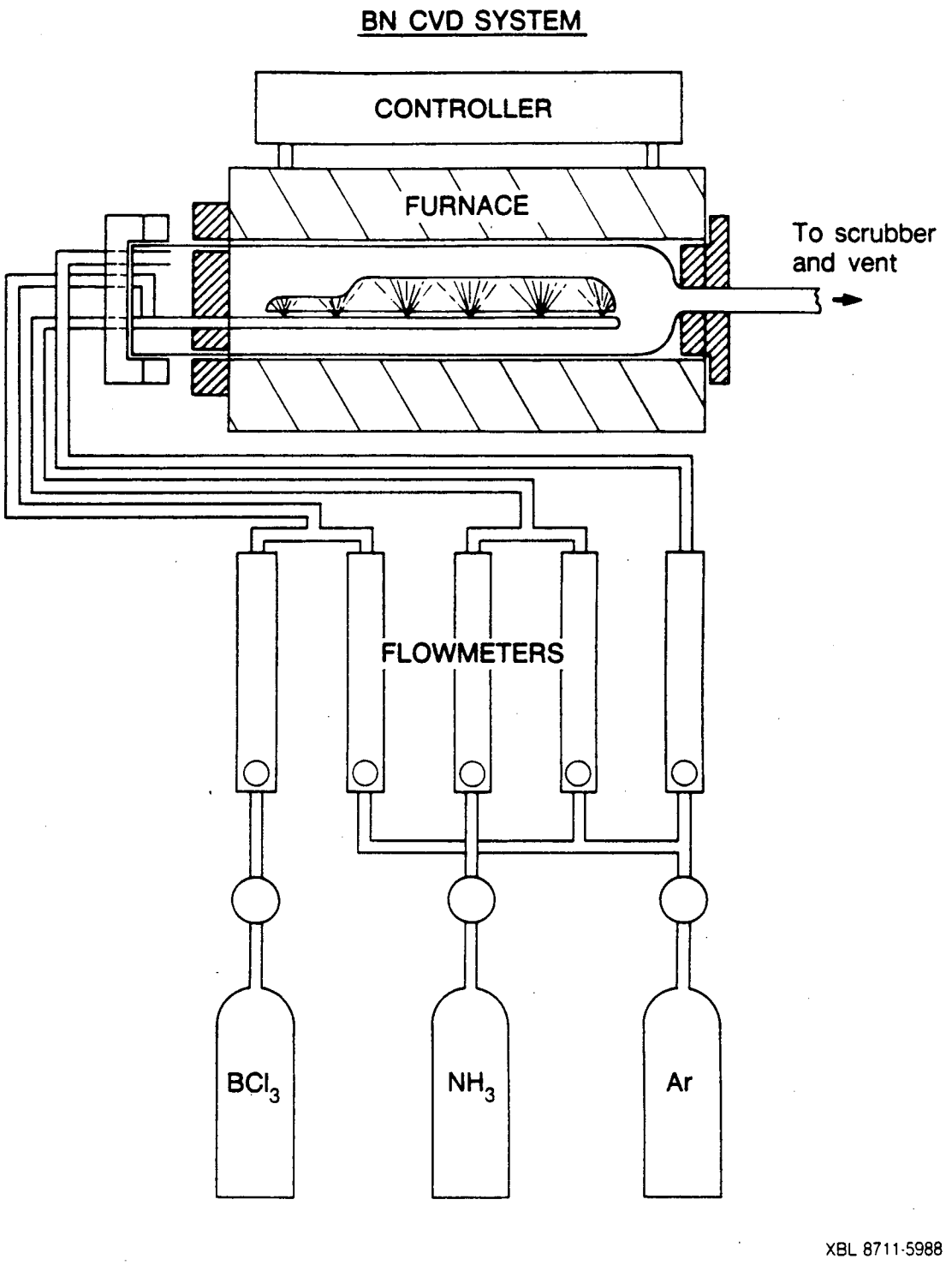

Figure 3 Schematic diagram of the chemical vapor deposition furnace used for boron nitride deposition on SiO_2.

material with and without the BN film. A Seeman-Bohlin diffractometer was used with Cu K_α (λ=1.54Å) radiation. Figure 4 is the resultant spectrum when the substrate spectrum was subtracted. A wide peak representing the (002) reflection of small grain hexagonal boron nitride is present. The apparent interplanar spacing derived from the position of the peak maximum is 3.72Å. A single broad peak was also observed for the amorphous films by Motijima et. al. (44) after annealing at 1000°C for 5 hr. The small grain size causes a broad peak that is shifted from the (002) reflection (3.33Å interplanar spacing) of crystalline BN. The crystallite size corresponding to the degree of line broadening seen for the (002) peak is calculated to be ~30Å using a correlation by Scherrer (47,48).

Optical absorption measurements utilizing a Perkin-Elmer Lamda-9 spectrophotometer revealed a sharp absorption edge for these films beginning at 0.21μm, corresponding to the 5.8eV direct bandgap of hexagonal BN (3,49).

Rutherford backscattering (RBS) of a 1.67 MeV He^+ beam with a of 165° backscatter angle yielded B and N peaks superimposed on the Si and O peaks (see figure 5). Films deposited on unabraded quartz show interference fringes indicating a film thickness near 1μm. The film thickness was confirmed by RBS to be ~1μm for a growth time of 15 min.

2.1.2.3 Synthesis impurities and arsenic pressure effects

Synthesis experiments were carried out using the materials and arsenic source temperatures listed in table 3. The following crucible materials were investigated: sandblasted SiO_2, Al_2O_3 cloth (Zircar AlW30A containing less than 1 percent SiO_2) in an SiO_2

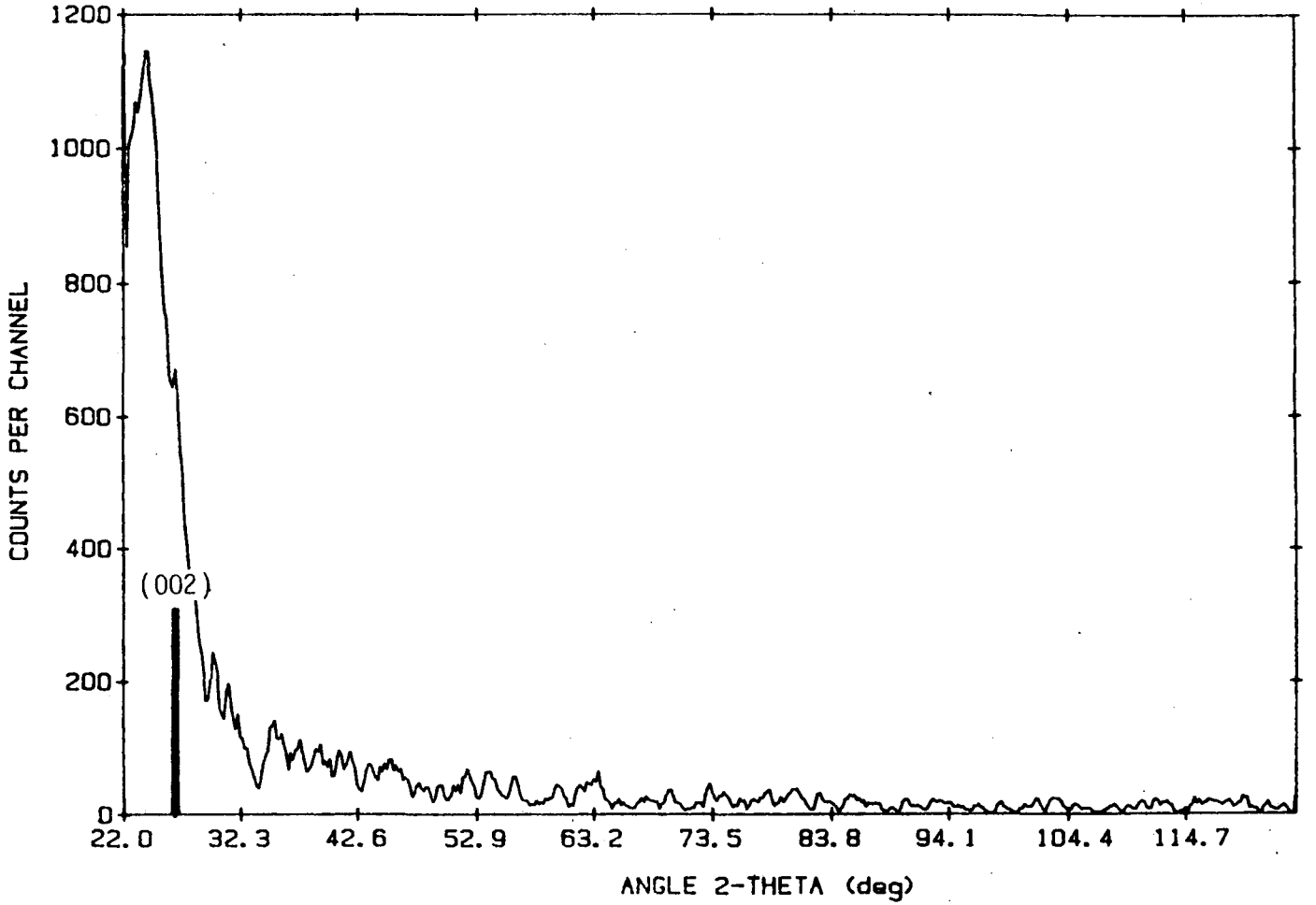

Figure 4 X-ray diffractometer spectrum of 1μm thick BN film.

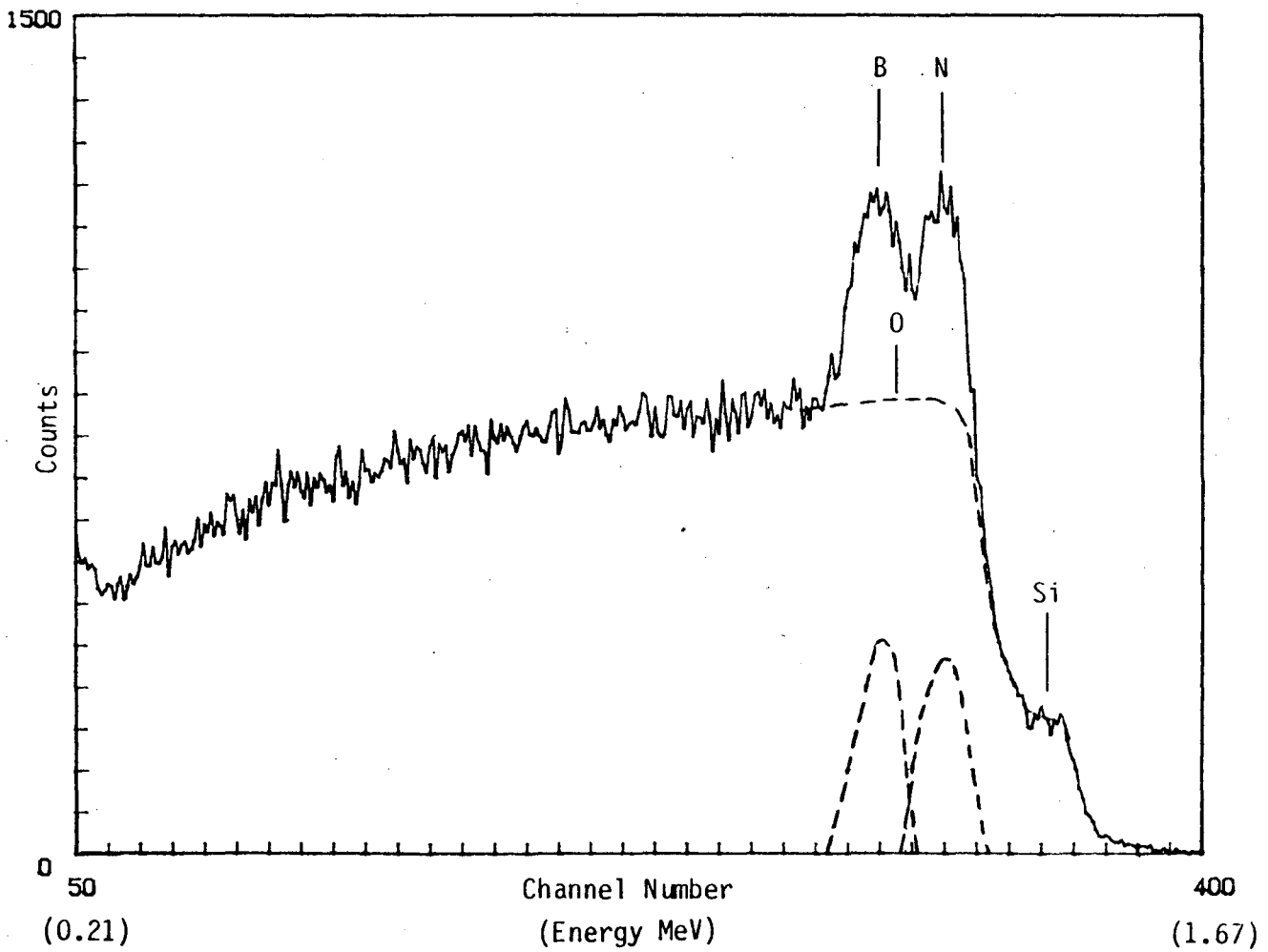

Figure 5 Rutherford backscattering spectrum of 1μm thick BN film.

Table 3. Impurity concentration and 300K Hall effect measurements for GaAs synthesized in a number of crucible materials. (continued in table 3a)

Material	Arsenic Temp. (°C)	N_D-N_A (cm^{-3})	Hall mobility (cm^2/Vsec)	ρ (ohm-cm)	θ	[EL2°]	SIMS* concentration [Si] (cm^{-3})	[C]	LVM [C_{As}] (cm^{-3})
1) SiO_2	620	6.1×10^{8}	970	1.1×10^{7}	>1(SI)	3.7×10^{16}	4×10^{15}	2×10^{16}	2.1×10^{13}
2) SiO_2	620	6.3×10^{15}	5600	0.176	0.65				
3) SiO_2	630	1.5×10^{15}	3300	1.3		6.9×10^{16}	7×10^{15}	1×10^{16}	
4) Al_2O_3	620	2.5×10^{7}	3500	7.2×10^{7}	>1 (SI)	3.5×10^{16}			9.8×10^{13}
5) BN film	620	9.6×10^{15}	4900	0.133	0.7				
6) Vit. C	618	9.0×10^{16}	230	0.30					
7) PBN	617	2.5×10^{15}	3800	0.77					
8) AlN	617	3.3×10^{15}	4200	0.65					
reference sample							2×10^{15}	6×10^{15}	

(SI) semi-insulating
*SIMS measurements by Charles Evans and Associates, Redwood City, CA

Table 3a. Additional SIMS analysis for two samples synthesised in SiO_2 at 620 and 630°C arsenic temperatures. (continuation of table 3)

Material	Arsenic Temp. (°C)	SIMS* concentration [O]	[S]	[Se]	[Te]
			(cm^{-3})		
1) SiO_2	620	$6x10^{16}$	$1x10^{15}$	$9x10^{13}$	$1x10^{14}$
3) SiO_2	630	$3x10^{16}$	$2x10^{15}$	$1x10^{13}$	$1x10^{14}$
reference sample		$2x10^{16}$	$1x10^{14}$	$2x10^{12}$	$8x10^{12}$

* SIMS measurements by Charles Evans and Associates, Redwood City, CA

crucible, CVD deposited BN film on an SiO_2 crucible, vitreous carbon, pyrolytic boron nitride, and aluminum nitride. The arsenic source temperatures and results of the synthesis experiments are listed in tables 3 and 3a. Results include: Hall effect measurements data, compensation ratio, the concentrations of Si, C, O, S, Se and Te from secondary ion mass spectroscopy (SIMS) for two samples, C_{As} from localized vibrational mode (LVM) spectroscopy for the two semi-insulating samples, and neutral $EL2^0$ concentrations measured by an optical absorption method following Skowronski (17). (This is the $EL2^0$ deep level concentration remaining after all net acceptors are compensated). The compensation ratio $\theta = N_A/N_D$ is defined here such that for p-type or semi-insulating GaAs, it will have a value greater than 1. For n-type GaAs, it can be found using net carrier concentration and mobility from a correlation based on mobility reduction due to ionized impurity scattering (50). This correlation can be used only when the Hall mobility is not defect-limited by

dislocations, grain boundaries, twins etc.

All samples measured were n-type semiconducting or n-type semi-insulating. Results indicate a carrier concentration $N_D-N_A<1x10^{16}cm^{-3}$ in all of the ingots except for the one synthesized in vitreous carbon. Two of the ingots were semi-insulating. Samples 1 and 2 of table 3 were grown under similar conditions, but sample 1 is semi-insulating and sample 2 is not.

Most of the synthesis samples have defect-limited mobilities. (Appendix 5.2 is a discussion of the effect of grain boundaries on mobility.) Consequently, only two θ values are stated in table 3 from this correlation and these may be greater than the true compensation ratios for these samples. The lowest θ was 0.65 for synthesis in SiO_2 with 620°C arsenic source temperature.

Carbon concentrations obtained by SIMS analysis of synthesis samples 1 and 3 and of two grown crystals to be presented in section 2.1.3.3. are questionable due to both a high SIMS background level for this impurity ($6x10^{15}$) and the low C_{As} concentrations obtained through LVM spectroscopy. Carbon on Ga sites (C_{Ga}) has not been detected by LVM and has been predicted to be less than 1 percent of the total [C] (51). The oxygen concentration measured for these samples is also questionable due to oxygen background levels that are close in magnitude to the oxygen concentration.

The semi-insulating Al_2O_3 synthesis sample was measured by Hall effect in the temperature range 295 to 321°C. An Arrhenius plot of N_D-N_A revealed a donor level at $E_C-0.724$ eV. This value is close to that of the $E_C-0.75$ eV ionization energy for EL2 measured by

DLTS (16).

The $EL2^{o}$ concentration of the synthesis sample grown with a 630°C arsenic source temperature was approximately two times that for those samples grown with a 620°C arsenic source temperature. This supports previous observations that EL2 concentration increases with excess As (16,52).

2.1.3 Silicon incorporation during growth

Silicon concentration in crystals grown in several crucible materials was measured in order to determine the relative rates for silicon incorporation in GaAs during growth. A method of calculating silicon incorporation rate is first presented. Growth in an SiO_2 cloth-lined crucible with a 617°C arsenic source temperature establishes a basis for incorporation rate comparison. The effect of arsenic temperature variation on the net carrier concentration is then presented for SiO_2 cloth-lined crucibles (T_{As}=613.5, 620°C), followed by results from growth in an Al_2O_3 cloth liner (T_{As}=620°C), in a graphite crucible (T_{As}=617°C), and in a vertical gradient freeze configuration of an SiO_2 crucible (T_{As}=617°C). In all cases to be considered, there is a large net flux (γ) of silicon to the melt as the crystal is growing that comes from either the crucible or the ampule.

2.1.3.1 Incorporation rate measurement

To determine the rate of silicon incorporation, a new equation for the impurity concentration will be derived using a few basic assumptions: 1) no solid diffusion, 2) complete mixing by convection in the liquid and 3) constant flux of new impurities. Consider the growth

of a volume element $A_i dx$ as in figure 6. The solute increase in the liquid is equal to the solute rejected to the liquid plus the new solute from the flux of new impurities:

$$A_i(L-x)dC_L = A_i(C_L-C_s)dx + (A_s\gamma/R)dx \qquad (2.1).$$

C_L and C_s are the concentrations in the liquid and in the newly grown solid respectively for a particular value of g, R is the growth rate, L is the crystal length, A_i is the growth interface area, and A_s is the area receiving the impurity flux. Dividing by $A_i L$ and setting x/L=g we find:

$$(1-g)dC_L = (C_L-C_s)dg + (A_s/A_i)(\gamma/R)dg \qquad (2.2).$$

Separating variables and integrating this expression from C_o (initial concentration in the liquid) to C_L and substituting $C_s = kC_L$ yields the following expression for C_s:

$$C_s = kC_o(1-g)^{k-1} + (A_s/A_i)(\gamma/R)(k/(1-k))[(1-g)^{k-1} -1] \qquad (2.3)$$

Substituting values for k=0.14 for silicon in GaAs (43), A_s, A_i, R and C_o, and knowing C_s and g from Hall effect measurements, yields values for γ for each measurement.

To find C_s, the concentration in the solid, we first assume the main impurity to be amphoteric silicon that is fully ionized with a

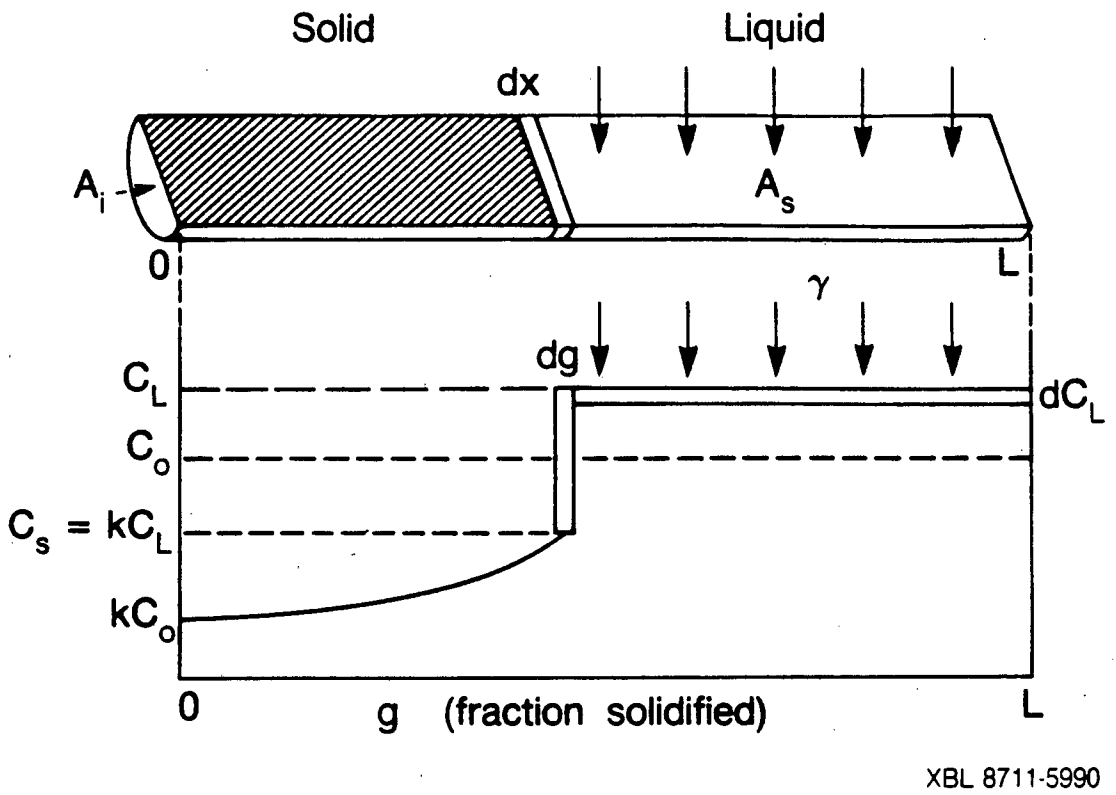

Figure 6 Schematic for the derivation of a normal freeze equation to include a constant impurity flux (γ).

fixed silicon concentration ratio:

$$r_{Si} = \frac{[Si_{As}]}{[Si_{Ga}]} \tag{2.4}$$

The total number of ionized donors and acceptors is that due to silicon (Si_{Ga} and Si_{As}) and non-amphoteric donors (d) and acceptors (a):

$$N_D = [Si_{Ga}] + [d] \tag{2.5}$$

$$N_A = [Si_{As}] + [a] \tag{2.6}$$

C_s is the total silicon concentration:

$$C_s = [Si] = [Si_{Ga}] + [Si_{As}] \tag{2.7}$$

Combining expressions 2.4 through 2.7 we now have an expression for C_s in terms of N_D-N_A:

$$C_s = [Si] = \frac{(1 + r_{Si})}{(1 - r_{Si})} ((N_D - N_A) + ([a]-[d])) \tag{2.8}$$

We now assume that for high silicon concentrations the difference ([a]-[d]) to be negligible compared to (N_D-N_A):

$$C_s \simeq \frac{(1 + r_{Si})}{(1 - r_{Si})} (N_D - N_A) \tag{2.9}$$

The value chosen for r_{Si} does not affect the relative comparison of silicon incorporation rates. We use r_{Si}=0.056 (7) for silicon incorporation comparisons so that:

$$[Si] = 1.12\ (N_D-N_A) \tag{2.10}$$

Equation 2.3 will be used in estimating the silicon flux (γ) from the room temperature Hall effect data for crystals grown from various crucible materials in the following sections.

2.1.3.2 Baseline incorporation - silica cloth-lined crucible

All seeded crystals in this work were measured along their length for net free carrier concentration (N_D-N_A), Hall mobility (μ) and resistivity (ρ) by room temperature Hall effect. Only N_D-N_A is reported here due to large variations in ρ and μ due to defect scattering. In each case, wafers were cut at intervals representing different amounts of the fraction solidified (g).

Figure 7 is a plot of N_D-N_A as a function of g for C17, a crystal synthesized in-situ and grown in an SiO_2 cloth crucible liner with a 617°C arsenic source temperature. The lower curve (equation 1.2) is a normal freeze distribution corresponding to the starting silicon concentration. There is an increase of carrier concentration above that explained by a normal freeze condition due to a silicon flux during growth. The silicon flux values corresponding to these measurements are in figure 8. The average incorporation rate is used to generate the upper curve fit (equation 2.3) to the data of figure 7. The average value of silicon flux was calculated to be $1.1 \times 10^{17} cm^{-2} hr^{-1}$. This will be the baseline crystal for further incorporation rate comparisons.

2.1.3.3 Arsenic pressure effects in silica cloth-lined crucibles

Two crystals were grown in SiO_2 cloth-lined crucibles with arsenic source temperatures above and below the optimum 617°C temperature of C17. Crystals C28 and C24 were grown with arsenic source temperatures 620°C (As-rich) and 613.5°C (Ga-rich) respectively. Synthesis in each case was carried out in a sandblasted SiO_2 crucible with the same arsenic source temperature as for

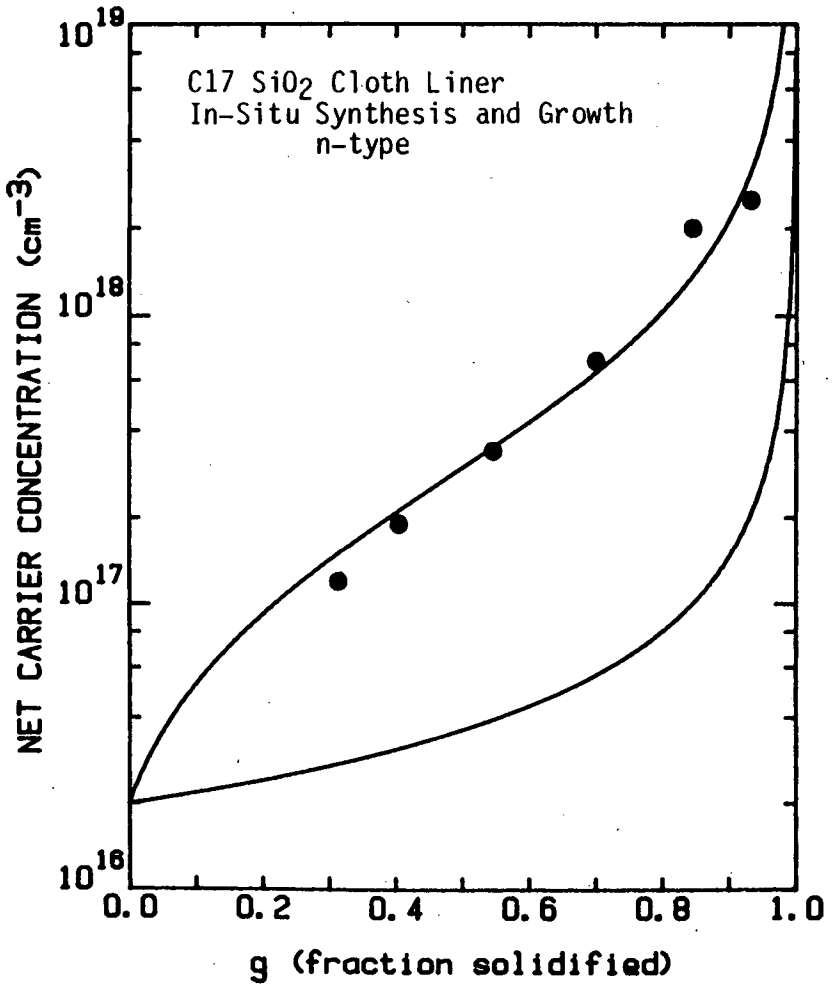

Figure 7 Free carrier concentration vs. fraction solidified (g) for a GaAs crystal grown in an SiO_2 crucible (T_{As}=617°C).

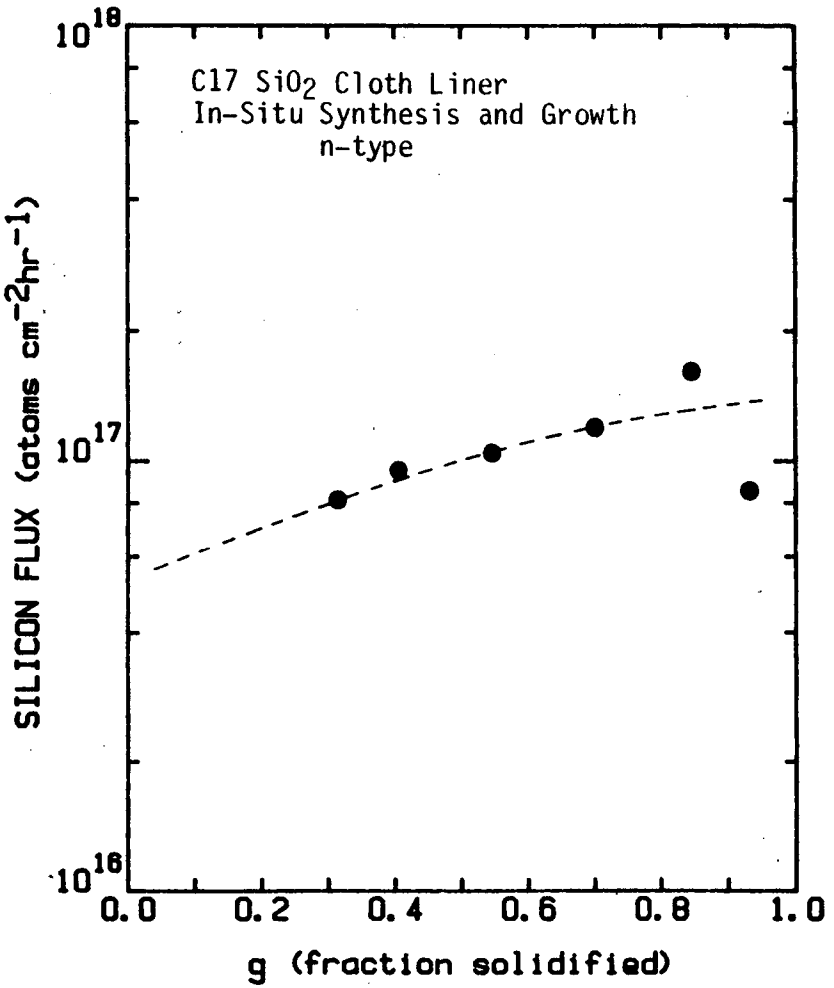

Figure 8 Silicon incorporation rate (γ) vs. fraction solidified (g) for a GaAs crystal grown in an SiO_2 crucible (T_{As}=617°C).

growth. The synthesis material for C28 was semi-insulating and sample 1 of table 3 was from this ingot. In figure 9, the carrier concentration is seen to increase at different rates for the two cases at different fractions solidified. For each Hall effect measurement, a corresponding flux (γ) was calculated. Figure 10 shows the incorporation rate variation with fraction solidified. At the start of growth the As-rich crystal received a greater flux of Si than the Ga-rich crystal. Both crystals approach the same incorporation rate as growth proceeds.

In addition, secondary ion mass spectroscopy (SIMS) analysis on two wafers from each crystal yielded data for the group IV impurities (carbon and silicon), and the first four group VI donor impurities (oxygen, sulfur, selenium and tellurium). Table 4 lists the SIMS analysis along with Hall effect measurements for the four samples.

$EL2^0$ concentrations measured by optical absorption were $1.5 \times 10^{16} cm^{-3}$ for C28 (As-rich) at g=0.34, and less than $5 \times 10^{15} cm^{-3}$ for C24 (Ga-rich) at g=0.43. This is indicative of the role of arsenic pressure in the appearance of the arsenic related defect responsible for EL2. An increase in arsenic atom fraction by increasing the arsenic source temperature has been seen to increase the concentration of EL2 (16,52).

2.1.3.4 Aluminum oxide cloth lined crucible

Crystal C27 was grown in an Al_2O_3 cloth lined SiO_2 crucible with a 620°C arsenic source temperature. The semi-insulating synthesis material used for this crucible was synthesized in SiO_2 with a 620°C arsenic source temperature, and its analysis was reported as sample 1

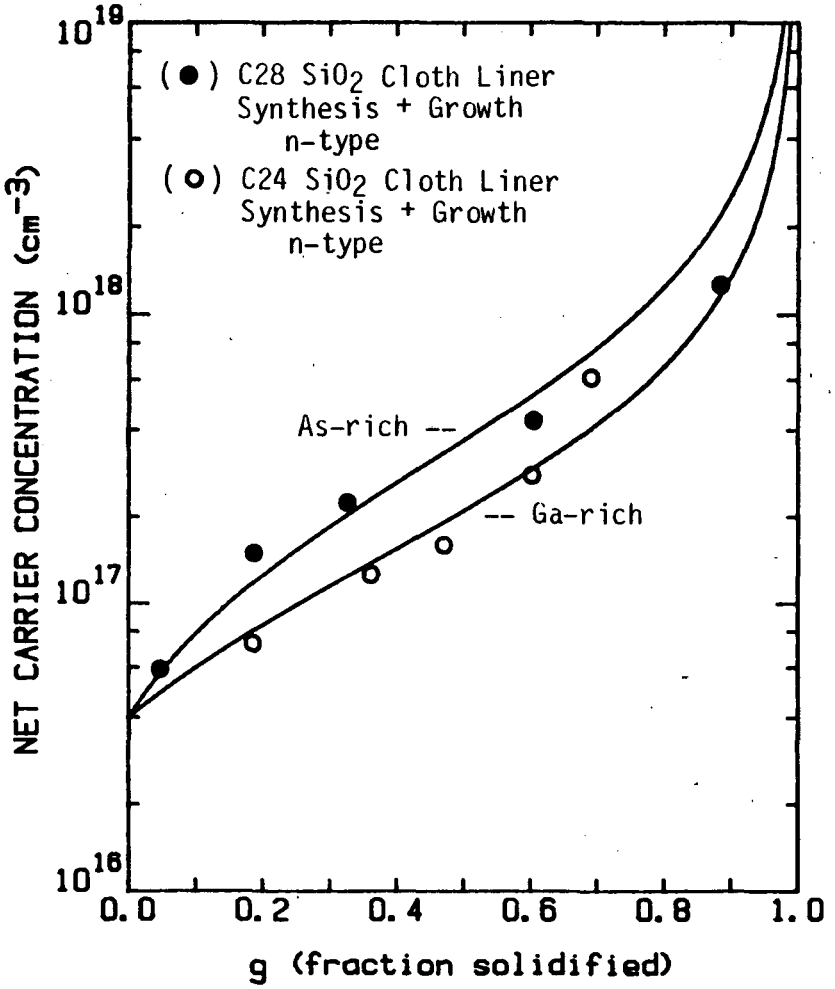

Figure 9 Free carrier concentration vs. fraction solidified (g) for two GaAs crystals grown in SiO_2 crucibles under arsenic-rich (T_{As}=620°C) and gallium rich (T_{As}=613.5°C) conditions.

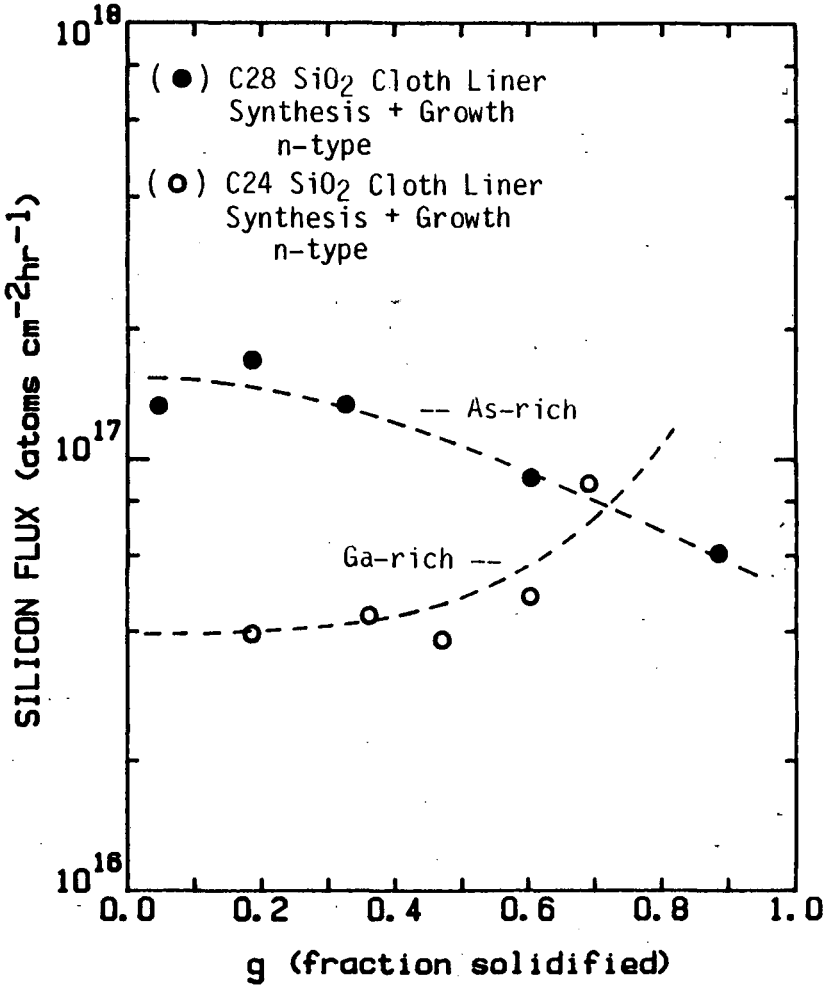

Figure 10 Silicon incorporation rate (γ) vs. fraction solidified (g) for two GaAs crystals grown in SiO_2 crucibles under arsenic-rich (T_{As}=620°C) and gallium rich (T_{As}=613.5°C) conditions.

Table 4. SIMS and Hall effect data for crystals C24 (Ga-rich) and C28 (As-rich) for low and high fractions solidified (g). Compensation ratio θ is calculated from carrier concentrations and mobility data using reference 50. The incorporation rate is the Si flux to the crystal calculated by solving equation 2.3 for each sample.

Sample	g	SIMS* concentration (cm^{-3}) Si	S	Se	Te	C	O	Hall Effect N_D-N_A (cm^{-3})	Compensation Ratio θ	Incorporation Rate γ ($cm^{-2}hr^{-1}$)
C24-1	0.186	$8x10^{16}$	$2x10^{15}$	$5x10^{12}$	$4x10^{13}$	$1x10^{16}$	$2x10^{16}$	$7.3x10^{16}$	0.5	$1.1x10^{17}$
C24-5	0.691	$1x10^{18}$	$1x10^{16}$	$7x10^{12}$	$8x10^{13}$	$6x10^{15}$	$3x10^{16}$	$6.1x10^{17}$	0.4	$2.4x10^{17}$
C28-1	0.047	$7x10^{16}$	$7x10^{14}$	$5x10^{13}$	$3x10^{13}$	$5x10^{15}$	$2x10^{16}$	$5.9x10^{16}$	0.7	$3.6x10^{17}$
C28-5	0.884	$2x10^{18}$	$1x10^{15}$	$8x10^{13}$	$4x10^{13}$	$1x10^{16}$	$3x10^{16}$	$1.3x10^{18}$	0.4	$1.6x10^{17}$
Reference Sample	--	$2x10^{15}$	$1x10^{14}$	$2x10^{12}$	$8x10^{12}$	$6x10^{15}$	$2x10^{16}$	---	---	---

--*SIMS measurements by Charles Evans and Associates, Redwood City, CA.

in table 2. Figure 11 is a plot of net free carrier concentration against fraction solidified for C27. Figure 12 shows the corresponding flux values for each carrier concentration measurement. The average flux, $5.0 \times 10^{14} cm^{-2} hr^{-1}$, is two orders of magnitude lower than those for SiO_2 crucibles. The crystal was n-type despite a reduction of silicon flux.

2.1.3.5 Graphite crucible

An in-situ synthesis and growth experiment was carried out in a carbon crucible (Poco DFP-1) with a 617°C arsenic source temperature. The crucible was first baked at 1000°C under vacuum to less than 1×10^{-5} Torr for 12 hours. The crucible was isolated during growth from contact to the SiO_2 ampule with BN supports to avoid a reaction of carbon with SiO_2.

The resulting crystal C23 was polycrystalline with a 1-3 mm grain size. Sticking of the crystal to the crucible was observed in the shoulder area. The body of the crystal did not stick to the crucible.

A plot of the net free carrier concentration against fraction solidified for crystal C23 is shown in figure 13 based on a constant $1 \times 10^{17} cm^{-3}$ carbon concentration due to crucible dissolution. The seed end of the crystal is p-type, presumably due to this carbon doping from the crucible. The position g=0.20 was found for the p to n type transition using a breakdown voltage profile (53) of a longitudinally cut slice of the crystal. At this position $N_{DD} + N_D$ from Si incorporation is greater than N_A and the crystal converts to n-type. A rapid influx of donor impurities is evidenced through the flux calculations shown in figure 14. At least a factor of three increase

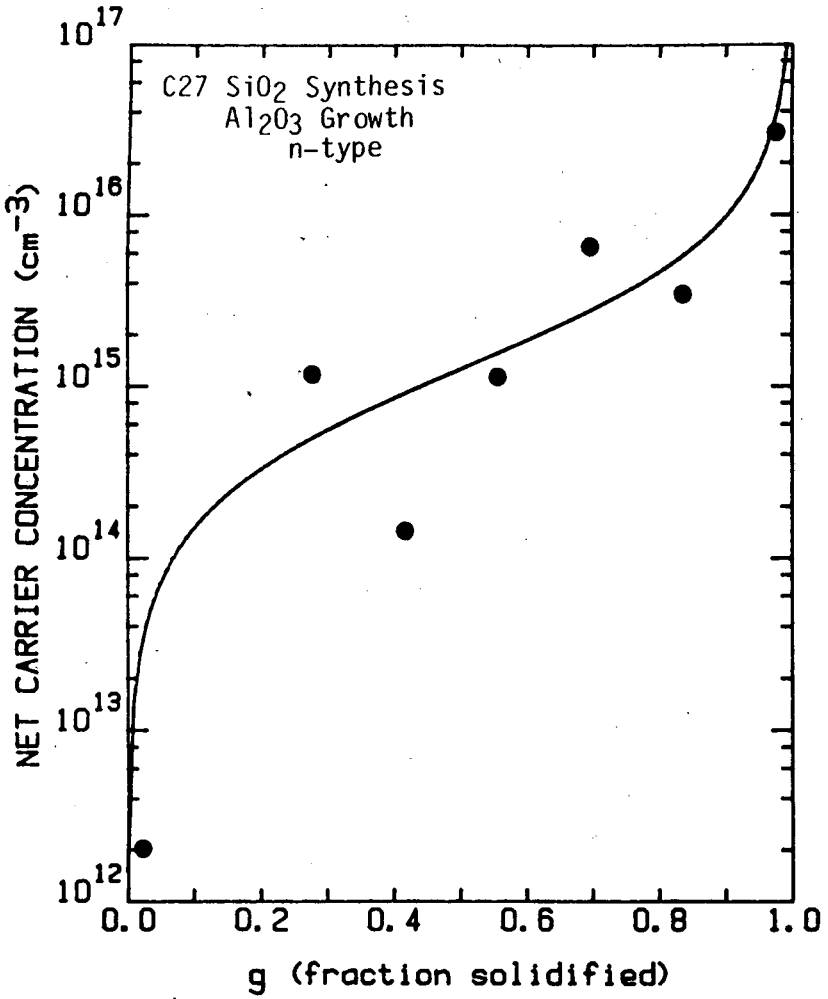

Figure 11 Free carrier concentration vs. fraction solidified (g) for a GaAs crystal grown with an Al_2O_3 crucible liner (T_{As}=620°C).

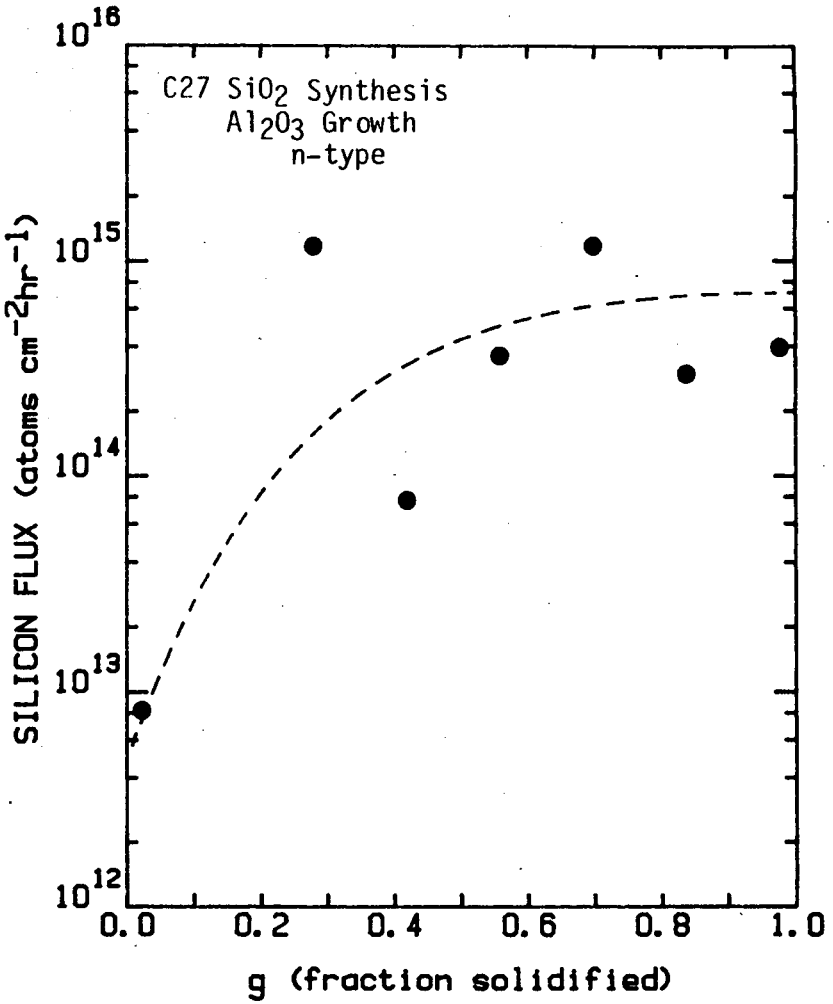

Figure 12 Silicon incorporation rate (γ) vs. fraction solidified (g) for a GaAs crystal grown with an Al_2O_3 crucible liner (T_{As}=620°C).

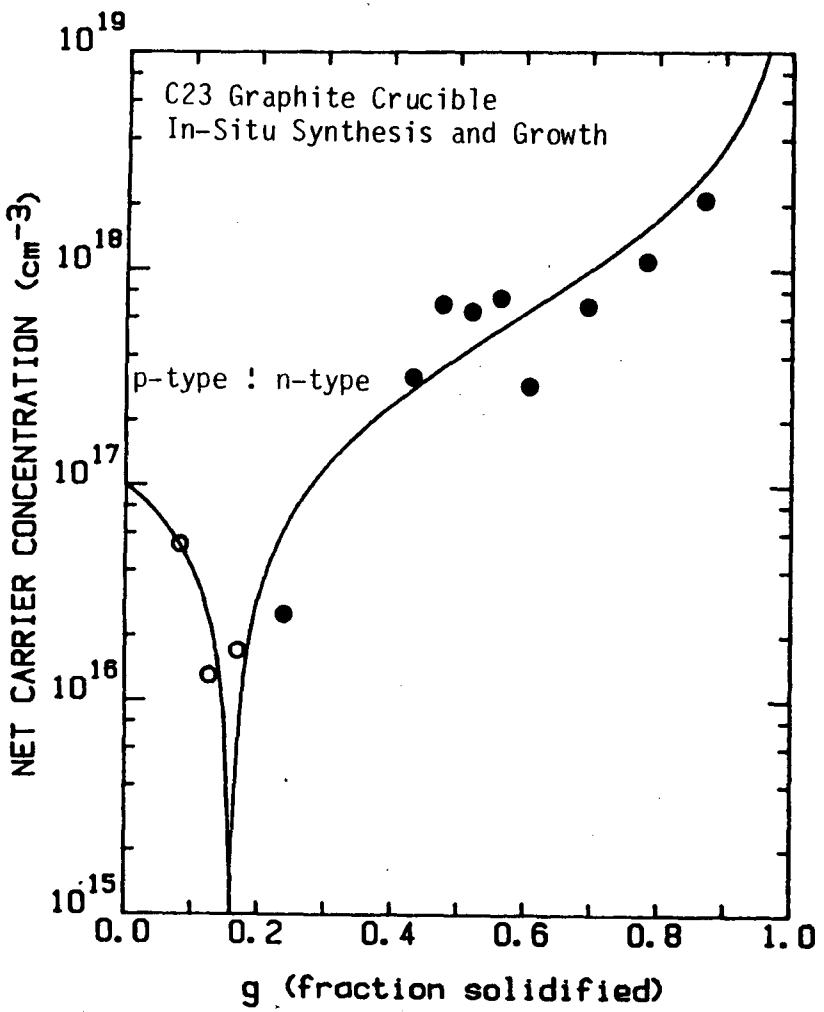

Figure 13 Free carrier concentration vs. fraction solidified (g) for a GaAs crystal grown in a graphite crucible (T_{As}=617°C).

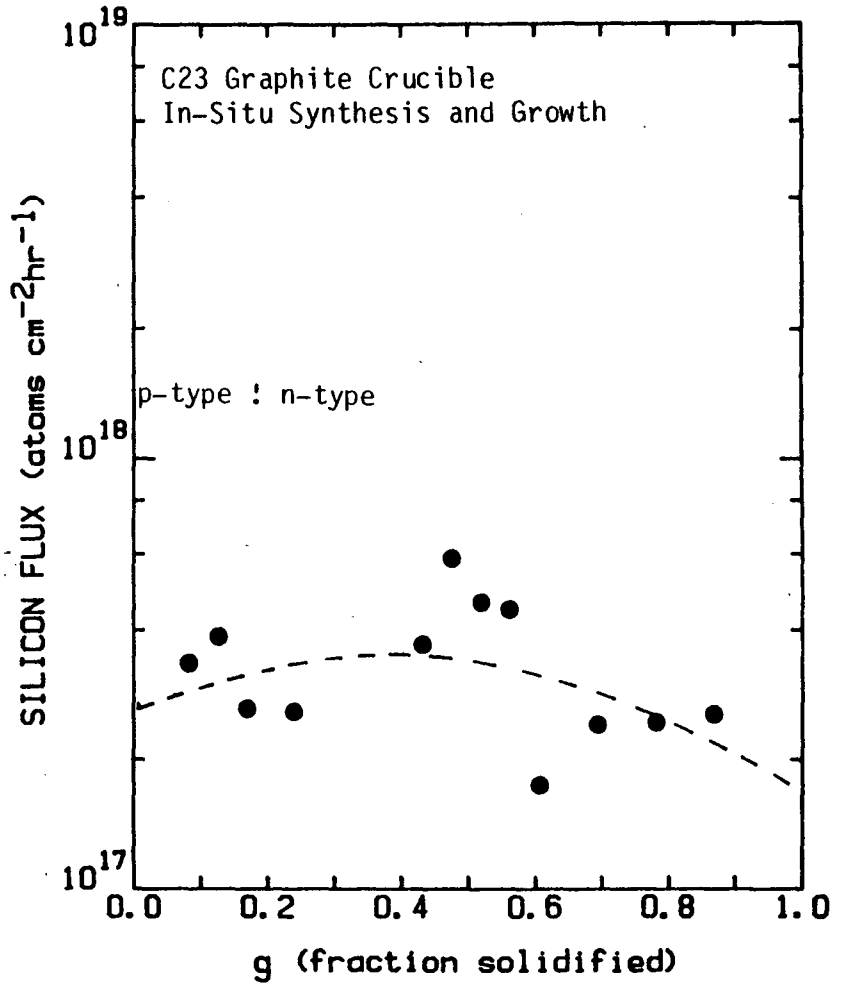

Figure 14 Silicon incorporation rate (γ) vs. fraction solidified (g) for a GaAs crystal grown in a graphite crucible (T_{As}=617°C).

is seen in silicon flux above that for the baseline crystal C17 grown in an SiO_2 crucible. When the incorporation of carbon acceptors with a k=1.0 segregation coefficient is included to the calculation along with the value g=0.2, we calculate average incorporation rates of at least $8x10^{15}cm^{-2}hr^{-1}$ carbon and $3.3x10^{17}cm^{-2}hr^{-1}$ silicon.
A further increase of silicon incorporation by a factor of three combined with an increase of carbon incorporation by a factor of 13 yields a very similar net carrier concentration profile. A more careful study would be required to determine the exact incorporation rates.

The longitudinally cut crystal was measured for neutral EL2 concentration ($EL2^0$) along its length by optical absorption at 1.1 μm relative to a 2 μm baseline absorption. The calibration for this measurement follows Skowronski (17). Figure 15 shows the variation of this concentration with fraction solidified. There is a strong dependency of [$EL2^0$] evident with carrier concentration (compare with figure 13). This is discussed in section 3.2.1.

2.1.3.6 Silicon incorporation in vertical gradient freeze growth

Two inch diameter GaAs crystals V1 and V9 were grown in a vertical configuration using pre-synthesized GaAs in a sandblasted SiO_2 crucible. The arsenic source temperature was 617°C. Through a similar analysis of net carrier concentration data as with horizontally grown crystals, silicon incorporation rates of $8.3x10^{15}cm^{-2}hr^{-1}$ and $1.6x10^{16}cm^{-2}hr^{-1}$ were obtained for V1 and V9 respectively. This is less than 1/7 the rate calculated for the analogous horizontally grown crystal C17.

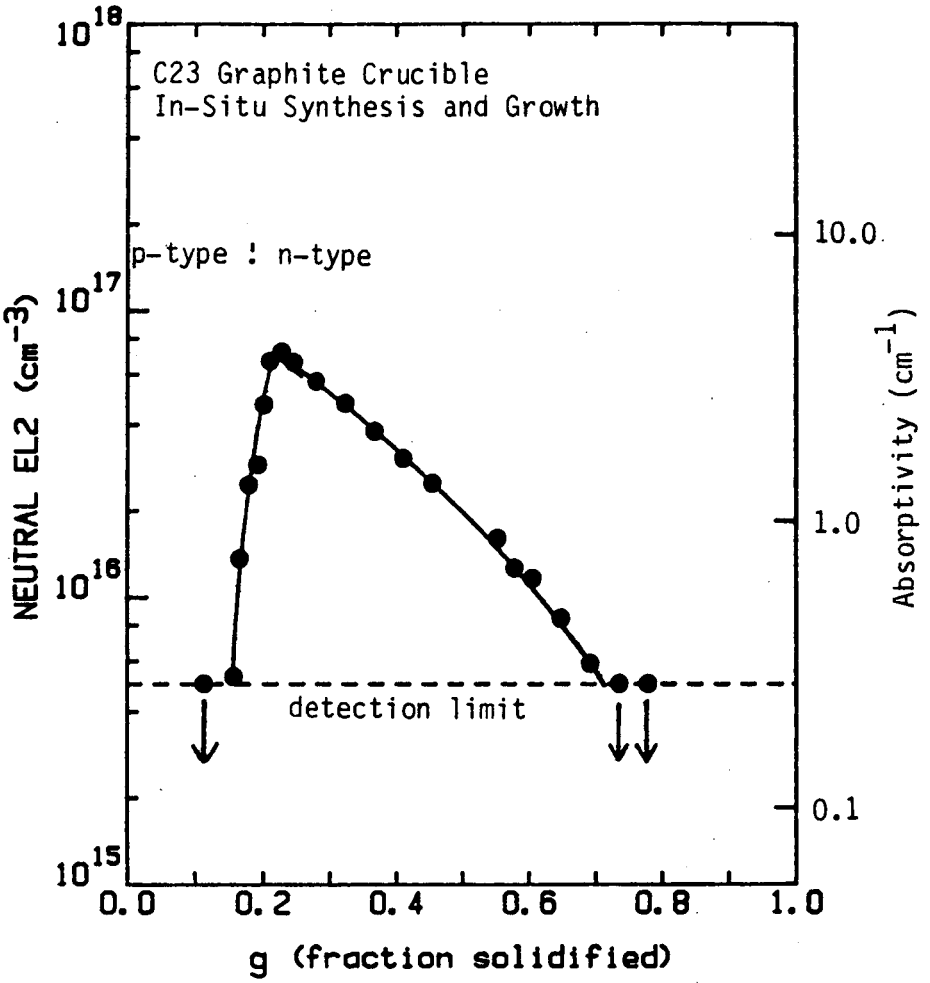

Figure 15 Neutral EL2 concentration by optical absorption at 1.1μm (300K) vs. fraction solidified (g) for a GaAs crystal grown in a graphite crucible (T_{As}=617°C).

2.1.3.7 Silicon incorporation rates - summary

Figure 16 shows the average incorporation rate of silicon for all crystals measured and discussed previously. Growth in various crucible materials shows a variation in incorporation rate of over three orders of magnitude. The variation of arsenic source temperature changes the incorporation rate within one order of magnitude. A discussion of these results follows in sections 3.2 and 3.3

2.2 Arsenic permeability experiments

The potential advantages of vertical gradient freeze growth of GaAs were discussed in section 1.3.3. The aim of this work was to explore the feasibility of the use of a graphite crucible in a vertical configuration by testing its permeability to As vapor and by estimating the degree of contamination of GaAs by carbon and silicon during synthesis in a closed graphite container. The permeability of graphite was tested to ensure the presence of arsenic vapor over the entire Ga melt surface for complete synthesis, and for the control of the crystal stoichiometry during growth. A graphite crucible could be coated with a liner such as BN to prevent carbon contamination in the crystal.

2.2.1 Graphite permeability

Arsenic permeability tests were carried out in a 12 in. long and 1.75 in. diameter Marshall model 2211 three zone tubular furnace insulated at both ends. The three zones were connected in parallel for effective operation as a single zone furnace. A thermal profile was obtained in a 100mm section of the furnace that was flat over the 300

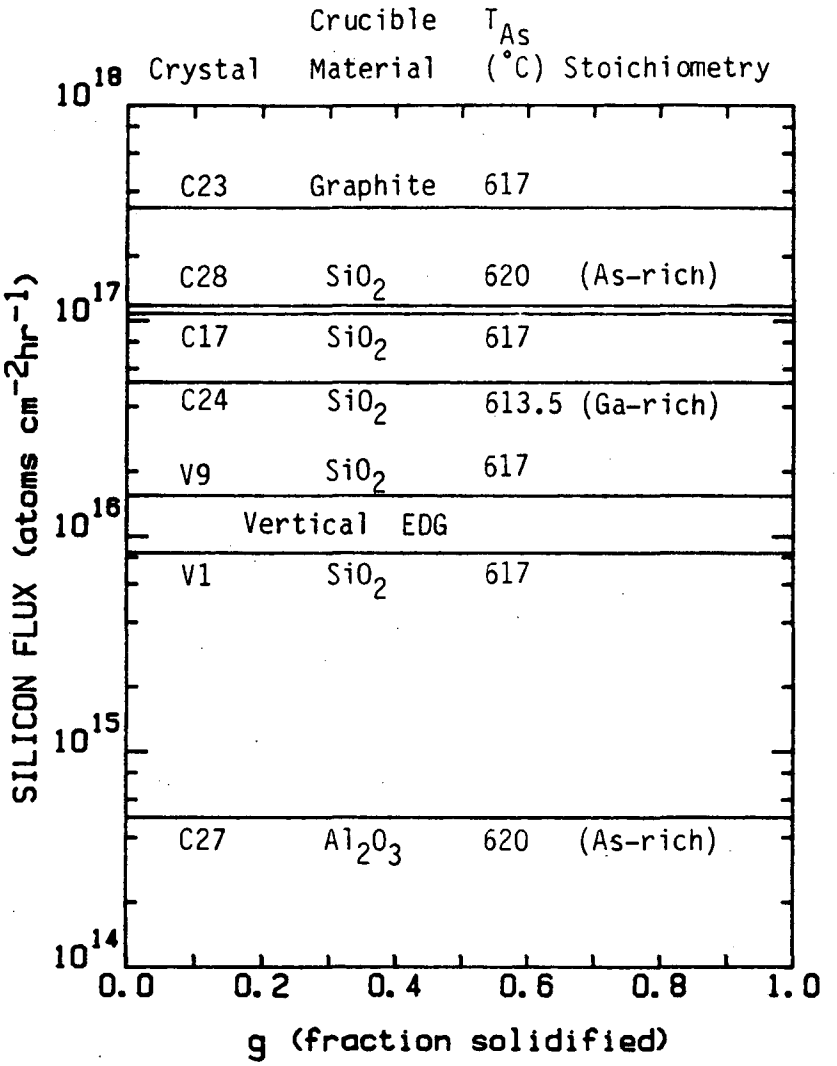

Figure 16 Average silicon incorporation rates (γ) for crystals grown in the indicated crucible materials.

to 600°C range to within ±10°C. A fused silica ampule was made from 42 x 45 mm tubing and was constricted to 4 x 6 mm tubing at one end in order to pass through the furnace insulation. This allowed a visual check for arsenic vapor condensation at the end of the tubing outside the furnace. A 100 mm x 19 mm diameter graphite container was filled with 1.9 g arsenic and sealed with a graphite threaded cap and Aquadag graphite suspension around the threads. Both the container and cap were Poco CZR-1 graphite. The container was then placed in the fused silica ampule that was then evacuated and sealed from the atmosphere. The container was then moved to the isothermal portion of the furnace and heated at 10°C/min to 400°C. This temperature corresponds to a 10^{-2}atm arsenic pressure. No condensate was seen at the ampule cold end. The container was heated again at 10°C/min to 500°C corresponding to an arsenic pressure of 0.1 atm. Arsenic condensation began at 460°C. The temperature was held at 500°C for 45 min. followed by cooling at 4°C/min. The weight of arsenic remaining in the container was compared to the starting amount resulting in a rate of a flow of 0.75 mg $cm^{-2}min^{-1}$ through the graphite wall at 500°C.

2.2.2 Synthesis in a sealed graphite container

Synthesis was then carried out according to the method previously discussed except the usual crucible was replaced with a Ga-filled and sealed graphite container in the high temperature section of the EDG furnace. The empty graphite container had been baked for 1 hr at 900°C with a pressure of <0.2 mTorr. The partially filled container was then placed on BN supports to isolate it from the SiO_2 ampule. The synthesis was carried out at an arsenic temperature of 617°C. The

resultant crystal inside the container was p-type GaAs with an average carrier concentration of $2.2 \times 10^{15} cm^{-3}$. Localized vibrational mode spectroscopy showed C_{As} absorption with a concentration of $3.3 \times 10^{16} cm^{-3}$. Assuming that only silicon amphoteric donors and acceptors in a concentration ratio of 0.056 (Si_{As}/Si_{Ga}) and that carbon acceptors were present, we arrive at a silicon concentration of $3.4 \times 10^{16} cm^{-3}$ (1.5 ppm).

In spite of the isolation of the graphite container from the SiO_2 ampule with BN spacers, a high concentration of silicon appears in the GaAs. A piece of the graphite used to make the container was found by emission spectroscopy to have 0.5±0.1 ppm silicon*. It is apparent that the silicon in the GaAs does not come from the container.

* Measured by Bruce Hart, Ultra Carbon Corporation

3.0 Discussion

3.1 Effects of crucible materials in synthesis

From the analysis of impurities in synthesized crystals presented in chapter 2, we can determine the requirements for semi-insulating GaAs in gradient freeze growth without the intentional addition of compensating acceptors. It is immediately apparent from the samples of table 2 that semi-insulating behavior in these crystals does not only depend on the arsenic source temperature and the crucible material. For example, samples 1 and 2 were synthesized in identical crucibles, and with the same arsenic source temperatures, yet sample 1 is semi-insulating and sample 2 is not.

We first determine the concentrations of the impurities that contribute to N_A, N_D, and N_{DD}. We then apply the 3-level compensation model (section 1.2.4) using the three defect concentrations. The impurity concentrations critical for compensation are the silicon concentration [Si], and the difference between the non-amphoteric ionized acceptor [a] and donor [d] concentrations. The following set of 5 equations, 5 dependent variables, and 4 independent variables describe the compensation in GaAs for these three concentrations:

$$r_{Si} = \frac{[Si_{As}]}{[Si_{Ga}]} \tag{2.4}$$

$$N_D = [Si_{Ga}] + [d] \tag{2.5}$$

$$N_A = [Si_{As}] + [a] \tag{2.6}$$

$$[Si] = [Si_{Ga}] + [Si_{As}] \tag{2.7}$$

$$\theta = \frac{N_A}{N_D} \tag{3.1}$$

When 4 independent variables are obtained from experimental data, the set of equations can be solved. For semi-insulating or p-type GaAs in this definition, the compensation ratio will have a value greater than 1. The net free carrier concentration in the semi-insulating case will be equal to the ionized deep level donors, N_{DD}^{+}, and cannot be used as N_D-N_A in the these equations.

Applying the first requirement for semi-insulating GaAs (N_A>N_D) to the above equations, an upper limit for silicon concentration is found:

$$[Si] < ([a] - [d]) \frac{1 + r_{Si}}{1 - r_{Si}} \tag{3.2}$$

For a given concentration of silicon and non-amphoteric donors, the concentration of acceptors needed to fully compensate all shallow donors is:

$$[a] > [d] + \frac{1 - r_{Si}}{1 + r_{Si}} [Si] \tag{3.3}$$

Applying the second requirement ($N_{DD}>N_A-N_D$), the lower limit for [EL2] is:

$$[EL2] \quad > \quad [a] - [d] - \frac{1 - r_{Si}}{1 + r_{Si}} [Si] \qquad (3.4)$$

The data for synthesis samples of table 2 were analyzed with the help of equations 2.4-2.7 and 3.1 to determine the remaining unknown concentrations. The upper limits for the silicon concentrations the samples can have without converting to n-type from semi-insulating, the total concentration of acceptors that are required to compensate the net donors, and the EL2 concentration required to compensate when $N_A>N_D$ were calculated using equations 3.2-3.4. The free carrier concentration for semiconducting GaAs is N_D-N_A. This and the measured compensation ratio, θ, are obtained from Hall effect measurements. The total silicon concentration, [Si], and donor (O, Se, S, and Te) concentrations, [d], are measured by SIMS. It is assumed that all donor impurity contribution [d] is due to the group VI elements. All silicon and group VI impurities are assumed to be substitutional and electrically active donors. It is also assumed that oxygen is a deep level donor impurity and is only partially ionized at room temperature due to a high ionization energy. Oxygen will only contribute significantly to the free electron concentration in semi-insulating crystals.

The value of r_{Si} was found by Hurle to depend on N_D-N_A (7) based on localized vibrational mode (LVM) measurements of Si_{As} and Si_{Ga} in highly doped horizontal Bridgman crystals (54, 55). This

work demonstrated a mass action law, self-compensation mechanism whereby where silicon atoms initially occupy the gallium site, but start occupying the As site as the free carrier concentration and Fermi-level increase. Beyond a concentration limit of $N_D-N_A \sim 5x10^{18}cm^{-3}$ (56), the formation of $Si_{Ga}-Si_{As}$ nearest neighbor pairs eliminates any further increase of carrier concentration (57, 58). The detection sensitivity for Si_{As} by LVM at 77°K was $\sim 2x10^{16}cm^{-3}$ (59), which limited the range of investigation to $N_D-N_A > 4x10^{17}cm^{-3}$. For $N_D-N_A < 10^{17}cm^{-3}$ a value of $r_{Si}=0.055$ is obtained by extrapolation of these data. We assume this value for synthesis sample calculations and confirm the low r_{Si} prediction using concentration data for low N_D-N_A samples in section 3.2.2

Table 5 lists the synthesis experiments with the measured or calculated values for [a], [d], [Si], N_D-N_A, θ, and [EL2°]. In section 2.1.1.2, we estimated the concentration of residual acceptors from the starting materials to be less than $1x10^{16}cm^{-3}$. The carrier concentration and SIMS data for sample 3 indicated in table 5 were used to determine its $6.9x10^{15}cm^{-3}$ residual acceptor concentration. This value was then used in the analysis of all other samples with the exception of samples 5 and 6, where the crucible was suspected of being a source of additional acceptor impurities. The $2x10^{15}cm^{-3}$ donor concentration used throughout the table (except for sample 5) was based on the higher of the two known concentrations of samples 1 and 3. Concentrations for two samples were estimated utilizing values for θ based on their semi-insulating behavior

Table 5 Dependence of semi-insulating behavior on residual acceptor, residual donor, silicon (r_{Si}=0.055), and $EL2^o$ concentrations for synthesis in different crucible materials and arsenic source temperatures. All concentrations are $x10^{15}cm^{-3}$ unless specified.

Crucible Material	Arsenic Temp. (°C)	n= N_D-N_A or N_{DD}^+	acceptors [a]	donors [d]	silicon [Si]	θ using ref.50	θ using eq. 3.1	[$EL2^o$]	Semi-insulating criteria [Si]<	[EL2]>	[a]>
		(x 10^{15} cm^{-3})						(x10^{15} cm^{-3})			
1) SiO_2	620	6.1x10^8	(7)	1.1	4		1.5	37	6.5	2.2-5.8	4.7
2) SiO_2	620	6.3	(7)	(2)	13	0.65	0.55		5.5	n.a.	13
3) SiO_2	630	1.5	6.9	2.1	7		0.82	69	5.4	n.a.	8.4
4) Al_2O_3	620	2.5x10^7	(7)	(2)	<5.5		>1.0	35	5.5	0-4.9	n.a.
5) BN film	620	9.6	n.a.	(>2)	<32	0.7	(<0.7)		n.a	n.a	n.a.
6) Vit. C	618	90	(>7)	(2)	>110		>0.12		n.a.	n.a.	>97
7) PBN	617	2.5	(7)	(2)	8.3		0.75		5.5	n.a	9.4
8) AlN	617	3.3	(7)	(2)	9.2		0.69		5.5	n.a.	10

___ measured value
( ) inferred from other measurements and used to calculate the remaining concentrations for this sample.
n.a. not applied in this case

(sample 4: $\theta>1.0$) and Hall effect measurements (sample 5: $\theta<0.7$). For semiconducting samples, the net free carrier concentration is the third quantity necessary to determine the remaining concentrations. The data for samples 4,5, and 6 were not sufficient to solve the equations, but in these cases upper or lower concentration limits were found.

Of the three ingots produced in SiO_2 crucibles, only sample 1 is semi-insulating. Sample 3 has nearly twice the [EL2°] of samples 1 and 4 due to its As-rich composition, but all three have more than 6 times the [EL2] required for semi-insulating behavior. The silicon concentration is clearly paramount in determining whether a given sample is semi-insulating; the value $[Si]=5\text{-}7\times10^{15}cm^{-3}$ is the upper limit for As-rich ($T_{As}>617°C$) crystals. To grow semi-insulating GaAs consistently, one must 1) eliminate silicon incorporation, or 2) compensate by $\sim1\times10^{16}cm^{-3}$ added acceptors, or 3) grow at precise stoichiometry where deep level acceptors are present to compensate silicon donors. For slightly Ga-rich crystals, a deep double acceptor level has been seen in LEC GaAs (52). The concentrations of both EL2 and the acceptor are $\sim1\times10^{16}$ at 0.0475 As atom fraction. The [EL2] is reduced as crystals become more Ga-rich, but a careful balance of stoichiometry would increase native acceptors without decreasing the [EL2] below the necessary $6\times10^{15}cm^{-3}$. If these native acceptors are present in gradient freeze GaAs, they could compensate $\sim1\times10^{16}$ silicon donors. The [EL2] in any case will not have to be greater than the residual plus native acceptor concentration.

Sample 4 grown in Al_2O_3 cloth was semi-insulating, with an estimated $[Si]<5.5\times10^{15}cm^{-3}$. Some silicon may be present from

dissolution of the Al_2O_3 cloth liner (1 percent Si), and through any silicon dissolved from the ambient vapor. Sample 5 contains $[Si]<3.2x10^{16}cm^{-3}$ based on upper and lower limits of [d] and θ, respectively, although this limit may be very high due to the uncertainty of θ. The BN film may contain doping impurities due to contamination from the BCl_3 (99.9 percent purity). Sample 6 grown in vitreous carbon was assumed to have an unknown concentration of carbon acceptors. The high free carrier concentration sets a lower limit of $[Si]>1.1x10^{17}cm^{-3}$. This is presumably aided by a vapor phase reaction between carbon and the silica ampule as suggested in section 3.2.1. Samples 7 and 8 both contain a relatively small concentration of silicon, but large enough to preclude semi-insulating properties.

With the exception of the sample grown in carbon, and possibly the sample grown in a BN coated crucible, the silicon content varies from $4x10^{15}cm^{-3}$ to $1.3x10^{16}cm^{-3}$ among the synthesized ingots. The reason for this is not clear, particularly considering that the two most extreme values are found in crystals 1 and 2 which were grown under identical conditions. The incorporation rate does not appear to be easily controlled at these concentration levels, but the calculated fluctuations may also be due to variations in residual acceptor and donor concentrations from their assumed values. Samples 7 and 8 would be expected to show significant reductions of silicon. The persistance of silicon incorporation despite the use of the isoelectronic crucible materials AlN and BN that do not contain SiO_2 is strong evidence of a mechanism where silicon is transported to the melt from the vapor phase. The source of silicon incorporation could be the ampule itself

through a mechanism involving a reaction of trace vapor impurities of arsenic vapor with the surrounding SiO_2 and subsequent transport of silicon to the melt. The application of the 3 level model with the assumptions of table 5 are sufficient to accurately predict semi-insulating behavior, and shows that only a slight reduction of silicon concentration ($2x10^{15}$ - $8x10^{15}cm^{-3}$) would have caused samples 2, 3, 7, 8, and possibly 5 to be semi-insulating.

3.2 Effects of crucible materials in growth

The effect of various crucible materials on incorporation of silicon during growth was shown in figure 16. Growth in graphite shows the highest value, followed by growth in SiO_2, and then in Al_2O_3. The incorporation rate for the Ga-rich crystal grown in SiO_2 was approximately 0.5 times that for both the As-rich crystal and the baseline crystal C17.

3.2.1 Graphite crucible

The 1.1 μm optical absorption of crystal C23 grown in carbon shown in figure 15 indicates the concentration of $EL2^o$ along the crystal length and through the p-n type transition. The concentration calibration is only approximate however due to variations in baseline absorption in the 1.1 to 2 μm region that are independent of the $[EL2^o]$ absorption. The source of this anomalous absorption is not known. For this reason, the apparent $[EL2^o]$ is high throughout the entire figure, and the [EL2] at high values of g decreases considerably more rapidly than is shown.

Figures 13 and 15 provide a graphic representation of the compensation mechanism in GaAs. The defect or defect complex responsible for EL2 is entirely compensated by carbon acceptors at the seed end and is in its positive charge state. The concentrations of residual acceptors and donors are negligible compared to the C and Si concentrations present in this crystal. Silicon is almost entirely on the gallium site for low free carrier concentrations. There is a net incorporation of silicon donors above that for carbon acceptors resulting in a compensation of the remaining acceptors and a decrease in carrier concentration. When $[Si_{Ga}^{+}] + 2[EL2^{++}] = [C_{As}^{-}]$, there is full compensation. From this point Si_{Ga} continues to incorporate faster than compensating acceptors, allowing them to release their electrons to the $EL2^{++}$ level. As more silicon incorporates, the $EL2^{++}$ level replaced by the $EL2^{+}$ level. When $[C_{As}^{-}] = [Si_{Ga}^{+}] + [EL2^{+}]$, this is the value of fraction solidified ($g \approx 0.17$) beyond which $EL2^{0}$ appears and the 1.1 μm optical absorption begins. This is the condition where we would expect the onset of semi-insulating conductivity. The $[EL2^{0}]$ increases until it is completely neutral at the full compensation condition $[Si_{Ga}^{+}] = [C_{As}^{-}]$ at $g \approx 0.20$. Beyond this point the crystal is n-type of carrier concentration $n = [Si_{Ga}^{+}] - [C_{As}^{-}]$. As n increases, a defect reaction occurs that reduces the concentration of the defect responsible for EL2 and the 1.1 μm absorption. The nature of this defect reaction is not known, but a defect reaction that correlates the free carrier concentration with an n^{-4} dependency was suggested by Lagowski (60). The baseline absorption obscures the magnitude of this

EL2 decrease.

Although silicon is present at ~0.5 ppm (see section 2.2.2) in the carbon crucible, this concentration could not be responsible for the high level of silicon incorporation observed in the crystal. The crucible was separated from the ampule during growth by BN supports to avoid a reaction between the carbon and the SiO_2 ampule. Silicon incorporation during the use of a graphite crucible may be explained if we assume 1) some dust from the crucible was exposed to the SiO_2 ampule leading to SiO_2 reduction or 2) gaseous products containing carbon outgassed from the crucible. The bakeout temperature of the carbon was limited to 1000°C, considerably less than the 1238°C growth temperature. Provided a minute quantity of carbon was in contact with to the ampule, silicon and carbon may enter the melt through the vapor phase by the following reactions (61):

$$SiO_2(s) + 2C(s) = Si(s) + 2CO(v) \qquad (3.5)$$

$$Si(s) + SiO_2(s) = 2SiO(v) \qquad (3.6)$$

The equilibrium partial pressures of SiO and CO calculated from reactions 3.5 and 3.6 at 1238°C are 9.6×10^{-4}atm and 1.3×10^{-2}atm respectively (61). Although wetting to the carbon crucible was minimal, carbon may also be incorporated through direct dissolution of the crucible. For the above reactions to apply to crystal C23, a mass of ~6 mg carbon would be required to react directly with the ampule in order to produce the quantity of silicon observed. A more likely

process for silicon incorporation involves a vapor transport reaction (62) such as the following:

$$SiO_2(s) + CO(v) = SiO(v) + CO_2(v) \qquad (3.7)$$

To drive this reaction, CO can be produced in the presence of oxygen as the transport agent either in the liquid or by a reaction with the solid carbon:

$$2C(sol) + 2O(sol) = 2CO(v) \qquad (3.8),$$

or,

$$2C(s) + O_2(v) = 2CO(v) \qquad (3.9),$$

where 'sol' signifies 'in solution'.

When the SiO(v) or $CO_2(v)$ is dissolved in the GaAs, oxygen is released to again combine with carbon producing CO(v). A set of vapor transport reactions of this type would explain the incorporation of silicon without the physical contact of carbon with SiO_2. The silicon incorporation for the crystal grown in graphite was >3 times the value for SiO_2 crucible growth indicating that a vapor incorporation mechanism is applicable. The silicon content of the vitreous carbon synthesis sample of table 5 was $[Si]>1.1\times10^{17}cm^{-3}$. The concentration for the sample synthesized in a closed graphite container (section 2.2.2) was $3.4\times10^{16}cm^{-3}$. These high values also indicate incorporation of silicon from the vapor phase, with a suppression of incorporation in the latter case due to the presence of

a graphite diffusion barrier surrounding the GaAs.

3.2.2 Silica crucibles

Silicon incorporation in SiO_2 crucibles was discussed previously utilizing equations 1.6 and 1.7 involving the reaction of the crucible with Ga(l) to dissolve SiO_2 producing $Ga_2O(v)$ which subsequently reacts with $As_4(v)$. The equilibrium vapor pressure of Ga_2O calculated from the equilibrium constant for the reaction (63) is 9.6×10^{-3} atm for the reaction of equation 1.5 at the melting point of GaAs. Table 6 shows an analysis of SiO_2 crucible grown crystals C24 (Ga-rich) and C28 (As-rich) using table 4 data and equations 2.4-2.7 and 3.1-3.4. A $7 \times 10^{15} cm^{-3}$ acceptor concentration obtained for synthesis results was assumed at the seed end of the crystal and is adjusted for normal freeze segregation using $k=10^{-4}$. This value (43) is the lowest segregation coefficient of all known values and hence allows a determination of an upper limit for residual shallow acceptors. The analysis for the two seed end samples follows that for table 5 except we now calculate r_{Si} and the remaining unknowns from [a], [d], [Si], and N_D-N_A. The silicon concentration ratio for the two tail end samples was obtained from the correlation by Hurle (7) for high carrier concentrations. This was combined with values for [d], [Si], and N_D-N_A. The calculation reveals acceptor concentrations greater than 5 times the values expected due to residual acceptors. These are assumed to be compensating native defects arising due to a mass-action law mechanism at high electron concentration during growth and cooling of the crystal. The acceptor concentration appears to increase with free carrier concentration, but no significant change is

Table 6 Dependence of silicon concentration ratio (equation 2.4) and compensation ratio (equation 3.1) on fraction solidified (g) for Ga-rich and As-rich crystals grown in SiO_2 crucibles. Limits of silicon concentration for semi-insulating behavior, and acceptor concentration needed to compensate shallow donors are also indicated for crystals near the seed end.

Sample	g	silicon [Si]	acceptors [a]	donors [d]	net carriers $n = N_D - N_A$	Compensation Ratio θ using equation 3.1	Silicon ratio r_{Si}	Semi-insulating criteria [Si]<	[a]>
			($\times 10^{15}$ cm^{-3})					($\times 10^{15}$ cm^{-3})	
C24-1 Ga-rich	0.186	80	(8.3*)	2.0	73	0.11	0.005	6.3	81
C24-5	0.691	1000	260 22*	10	610	0.35	(0.074)	n.a.	n.a.
C28-1 As-rich	0.047	70	(6.9*)	0.78	59	0.14	0.036	6.6	66
C28-5	0.884	2000	320 59*	1.12	1300	0.28	(0.105)	n.a.	n.a.

___ measured value
* Upper limit calculated based on $k=10^{-4}$ with 6.9×10^{15} cm^{-3} initial concentration.
( ) inferred from other measurements and used to calculate the remaining concentrations for this sample.
n.a. not applied in this case

seen due to differences in arsenic source temperature.

The average silicon incorporation rate for the crystal grown in Ga-rich conditions is approximately 44 percent of that for the crystal grown in As-rich conditions (see fig. 16). The incorporation rate for the As-rich crystal decreases while that for the Ga-rich crystal increases. The silicon concentration ratios in the two crystals are less than 0.04 near the seed and 0.09 near the tail. The seed end values are very close to the r_{Si}=0.056 theoretical extrapolation used in table 5 for synthesis crystals with low free carrier concentrations. The tail end values were taken from a study of a large number of horizontal Bridgman GaAs crystals that showed no evidence of significant Si_{As} occupation below a net carrier concentration of $10^{18}cm^{-3}$. The different incorporation rates therefore cannot be explained by a stoichiometry dependent site preference of the silicon atoms. The difference in arsenic pressure calculated from the arsenic vapor equilibrium pressure and temperature diagram (43) for the two temperatures is ~5 percent; the silicon incorporation rate is higher for the larger pressure case where we would look for a higher apparent incorporation due to a high occupation of Ga sites by silicon. The values obtained for r_{Si} from table 6 do not show a difference between the two crystals that would support this.

A mechanism involving vapor diffusion rate differences (see eq. 1.6 and eq. 1.7) of Ga_2O from the melt would predict a higher incorporation rate in the Ga-rich crystal due to a reduced arsenic pressure. Also diffusion of any silicon from the vapor would tend to increase at lower arsenic pressures.

The incorporation rates for the As-rich crystal and for the baseline crystal C17 are nearly identical. The reduced incorporation rate in the Ga-rich case could be a virtual effect due to the compensation of incorporated silicon by deep level acceptors. The presence of a double acceptor in Ga-rich LEC GaAs crystals has been observed at 0.07 and 0.18 eV above the valence band (52). We suggest a defect reaction mechanism that creates new acceptors, compensating some of the silicon donors as the carrier concentration increases. A likely reaction considering the stable charge states for defects (10) in n-type crystals is the following (14):

$$V_{As}^{+} + 6e^{-} = Ga_{As}^{-2} + V_{Ga}^{-3} \qquad (3.10).$$

This reaction depends on a high concentration of arsenic vacancies to proceed. These can be provided by the arsenic pressure deficiency at T_{As}=613.5°C. The relevant reaction is (43):

$$1/4\ As_4(v) + V_{As} = 0 \qquad (3.11).$$

The appearance of acceptors would increase rapidly with carrier concentration, and decrease with increased arsenic pressure. The exact solution for the defect equilibrium would require a consideration of all defects with significant concentration and their true charge states, as well as the values of the respective equilibrium constants at the temperature where the concentrations become fixed during cooling. A reaction similar to equation 3.10 would explain the

presence of compensating acceptors seen for the two high carrier concentration samples in table 6. However it does not explain the apparent reduction of silicon incorporation for the Ga-rich crystal. The As-rich and Ga-rich crystals have very similar values of compensating acceptors.

One remote possibility to explain the differences of incorporation is a variation of the segregation coefficient for silicon with crystal stoichiometry. The presence of less $[V_{Ga}]$ may decrease the incorporation of silicon in the Ga-rich crystal during growth (decreased k_{Si}), yet not affect r_{Si}. The r_{Si} ratio may reach an equilibrium value at a different temperature during cooling, depending more on the carrier concentration than the stoichiometry.

3.2.3 Alumina crucible

For growth in Al_2O_3, the silicon incorporation was two orders of magnitude less than for growth in SiO_2. The net carrier concentration was below $10^{16}cm^{-3}$ for 90 percent of the crystal length. Dissolution of Al_2O_3 in molten Ga was described by Cochran and Foster (63) using the following reaction:

$$4Ga(l) + Al_2O_3(s) = Al_2O(v) + 2Ga_2O(v) \qquad (3.12).$$

These authors observed a very low reactivity of Al_2O_3 with Ga relative to that of SiO_2 with Ga. Thermodynamic calculations at the 1511 K melting point of GaAs indicate a ΔG_r for equation 3.12 of 59.8 kcal/mole compared to 26.9 kcal/mole for equation 1.6 (SiO_2 dissolution in Ga) and 26.0 kcal/mole for equation 3.5 (carbon-SiO_2

reaction). Since we expect Al_2O_3 to be less reactive than SiO_2 with Ga, and we also know the concentration of SiO_2 in the Al_2O_3 is <1 percent, we conclude the majority of silicon is not reaching the melt from the crucible, but primarily through the vapor phase. The magnitude of this incorporation rate is below the $5.0 \times 10^{14} cm^{-2} hr^{-1}$ incorporation rate of the crystal grown in Al_2O_3. The incorporation rate derived in section 2.1.3.1 is not specific to incorporation from the crucible, but reflects silicon (net free carrier) incorporation from any source. This vapor phase incorporation would also be expected to occur for growth in other crucible materials, and explains the existence of silicon concentrations in the synthesis samples of section 3.1 irrespective of the crucible material used.

3.3 Silicon incorporation during vertical growth

Vertical gradient freeze growth is different from horizontal growth in regard to silicon incorporation. The melt is contained within the crucible, exposed to the vapor ambient only at the top. The vertical thermal gradient reduces the melt convection that may be responsible for the transport of silicon to the growth interface in horizontal growth. Silicon incorporation is more limited by diffusion in this case. These factors combine to reduce the silicon incorporation by an order of magnitude from that for growth in horizontal crucibles under similar growth conditions.

4.0 Summary and conclusions

The application of equations 2.4-2.7 and 3.1-3.4 describing compensation by the 3 level model for the synthesis ingots of section 3.1 leads to a number of important conclusions. The analysis, using SIMS and Hall effect data allows the determination of the relevant electrically active impurity concentrations or ratios [a], [d], N_D (or N_A), N_D-N_A, Si, Si_{Ga}, Si_{As}, r_{Si}, and θ provided 4 of these quantities can be measured or estimated. A residual acceptor $[a]=7x10^{15}cm^{-3}$ and donor $[d]=2x10^{15}cm^{-3}$ concentrations were found in synthesis ingots which enabled the analysis to be carried through knowing only N_D-N_A for other samples. The concentrations [a] and [d] were assumed to originate from the starting materials, primarily the arsenic, and therefore were expected to follow the normal freeze equation without new incorporation during growth. Analysis of a number of synthesis crystals led to the conclusion that to have semi-insulating behavior in gradient freeze GaAs, $[Si]<4x10^{15}$ is required. This means that the incorporation of silicon is the primary obstacle. The presence of more than 6 times the [EL2] required to compensate residual acceptors in As-rich ingots indicates the reduction of [Si] will allow semi-insulating behavior. Silicon incorporation is not exclusively dependent on the dissolution of SiO_2 in contact with the melt, but the melt contains some silicon incorporated from the vapor that is responsible for a silicon concentration $[Si]\sim10^{15}$ in all synthesis ingots.

A method to determine the relative silicon incorporation rates

either from crucible dissolution or from the vapor was derived from a modification to the normal freeze equation. The incorporation rates, measured as a function of fraction solidified for six gradient freeze crystals, revealed orders-of-magnitude differences for carbon, SiO_2, and Al_2O_3 crucibles. Silicon incorporation for growth in a carbon crucible is seen to involve a vapor-solid reaction between the carbon of the crucible and the surrounding SiO_2 ampule resulting in a high incorporation rate relative to the baseline crystal grown in SiO_2. A contributing factor to this high level of incorporation may have been the presence of carbon in vapor outgassed from the carbon crucible. A vapor transport reaction involving oxygen as the transport agent would explain the lack of detectable reaction products other than silicon. Carbon incorporation was also seen, but at a lower rate, the two combining to create a p to n type transition. Growth in an Al_2O_3 crucible showed that silicon incorporation from the vapor is less than 10^{-2} times that for crucible dissolution when growth is carried out in SiO_2. This implies that irrespective of crucible material, it will be necessary to reduce the incorporation of silicon from the vapor phase prior to growing semi-insulating GaAs in closed ampules. Growth in silica crucibles at three arsenic source temperatures revealed a slight reduction of the average silicon incorporation rate in Ga-rich crystals. Also the incorporation rates were seen to increase with fraction solidified for Ga-rich crystals and to decrease in As-rich crystals. The reasons for these variations are unknown, but they are small in comparison to the effects of the different crucible materials. Silicon incorporation during growth in a vertical

configuration was an order of magnitude less than that for horizontal growth due to reduced convective mixing and reduced melt-vapor contact area.

SIMS and Hall effect impurity analysis of the As-rich and Ga-rich crystals grown in SiO_2 revealed native acceptor concentrations 2.6 and $3.2 \times 10^{17} cm^{-3}$ corresponding to the free carrier concentrations $N_D - N_A = 6.1 \times 10^{17}$ and $1.3 \times 10^{18} cm^{-3}$ respectively. These acceptors appear to be compensating point defects with a concentration related to the free carrier concentration during growth and cooling. The acceptors were not observed in either the As-rich or Ga-rich crystals at low $N_D - N_A$. The low acceptor concentration in a low carrier concentration Ga-rich seed end sample suggests that the stoichiometry related native acceptor seen in Ga-rich LEC crystals is not present in gradient freeze crystals.

Crystals C24 and C28 showed even lower r_{Si} than predicted from the theoretical extrapolation $r_{Si} = 0.056$ for low $N_D - N_A$. The impurity analysis technique developed here may therefore prove useful in calculating $[Si_{As}]$ when its concentration is below LVM detection limits, or cannot be seen by LVM due to free carrier absorption.

We suggest further SIMS analysis of synthesis ingots to allow the evaluation of precise residual acceptor and donor concentration variations among growth runs due to impurities from the arsenic, and from the crucible materials.

Further work to achieve semi-insulating GaAs in gradient freeze growth should include growth in a BN coated or an Al_2O_3 lined crucible in a vertical configuration. This will allow calculation of

the relative incorporation rate to determine the extent of vapor incorporation of silicon. The absence of SiO_2 in the crucible, and the reduced surface area exposed to vapor will most likely result in semi-insulating properties for the crystals. If silicon incorporation through the vapor cannot be adequately reduced through this method, the use of an ampule liner material such as boron nitride not containing silicon would further reduce the vapor incorporation. This would avoid the exposure of SiO_2 at the growth temperature to the growth environment should the applicable vapor transport reaction contain vapors condensable below the growth temperature. The BN coating process may be useful to achieve an inert liner, although it may weaken the quartz at high temperatures by introducing boron impurity to the SiO_2. The use of a methanol rinse for cleaning the ampule and crucible prior to growth should be avoided in light of the high silicon incorporation rates for crystals grown in the presence of carbon. Vertical gradient freeze growth using a graphite crucible with a BN coating would bring As vapor to the melt surface for in-situ synthesis and stoichiometry equilibration, prevent the direct contact of the melt with carbon, and create a diffusion barrier to silicon incorporation from the vapor.

5.0 Appendix

5.1 Procedure for making ohmic contacts on bulk GaAs for Hall effect

1. Cut a ~1 mm thick slice.

2. Lap sample with 3μm Al_2O_3 (prior to polishing) or 600 grit SiC.

3. Wax sample to polishing block and polish with 1:1:1 Syton colloidal silica:H_2O_2:H_2O for 2 hours.

4. Swab sample with trichloroethylene to remove all wax residue.

5. Rinse well with acetone, then de-ionized water.

6. Etch sample with HCl for 1 min, then 3:1:1 H_2SO_4:H_2O:H_2O_2 for 2 minutes while agitating or stirring to prevent bubble formation. The 3:1:1 solution must be freshly prepared.

7. Cut four small pieces of InSn alloy for n-type or n-type semi-insulating contacts, or InZn alloy for contacts to p-type material.

8. Just prior to pressing the contacts to the sample, both the sample and the contact metal must be etched in HCl to remove any residual surface oxides.

9. Press the alloy on to the corners of the sample with tweezers to make good surface contact.

10. Heat sample under inert gas for 10 min. at 400°C (n-type), or 200°C (p-type). Cool under inert gas.

11. Test for ohmic contacts with an ohmmeter. An I-V curve trace is useful to verify suspected rectifying contacts. In general poor contacts are an indication of inhomogeneity of the material. If all procedures are followed correctly and the alloy is correct for the electrical type, it is seldom advantageous to repeat the contact procedure on the same sample.

12. Use a clean, low temperature soldering iron to solder wires to the sample.

Steps 3 and 4 may be omitted without significant change in the contact quality.

Appendix

5.2 Effect of grain boundary on carrier concentration and mobility

Hall measurements performed on polycrystalline samples made it necessary to evaluate the effect of grain boundaries. It was observed that mobilities measured on samples containing grain boundaries varied widely. To the contrary, net carrier concentrations were less dependent on grain boundaries, dislocation density or other sample inhomogeneities. An n-type GaAs sample with a clearly defined grain boundary was measured by Hall effect using two ohmic contacts on each side of the boundary. The contacts were removed, the sample was then cut along the grain boundary. The two single grains were then lapped and prepared for Hall measurements. The results shown in table A-1 reveal that although the measured carrier concentrations for all three samples agree within 25 per cent, there is nearly an order of magnitude difference in measured mobility and resistivity values. The anisotropy factor varies by at least 3 orders of magnitude. This is easily understood since carrier concentration would not be expected to vary considerably in the bulk due to the influence of a grain boundary. Mobility and consequently resistivity across a grain boundary could be affected by non-isotropic electrical effects such as electrical fields due to accumulated charged impurities that segregate to the boundary during growth.

Appendix

Table A-1

	N_D-N_A cm^{-3}	μ cm^2/Vs	ρ ohm-cm
Grain boundary sample	1.27×10^{17}	442	0.129
Single grain sample 1	1.57×10^{17}	3270	0.0122
Single grain sample 2	1.43×10^{17}	3160	0.0138

When possible, Hall measurements in this work were made on single grains. Some crystals did not remain a single crystal throughout growth. Others were polycrystalline from the start e.g. C23 and C27. The large amount of scatter in net carrier concentration is seen in the latter two crystals, and is attributed to inhomogeneities in the sample. Mobility values for most samples measured were much lower than would be expected for entirely homogeneous samples. For this reason, the calibration of reference (50) will in general only give an upper limit for the compensation ratio.

6.0 References

1. P.H. Singer, Semiconductor International, Nov. 1986.

2. A.S. Grove, "Physics and Technology of Semiconductor Devices", J. Wiley and Sons, 1967.

3. Landolt-Bornstein, "Numerical Data and Functional Relationships in Science and Technology", Group III, V.17a, Ed. O. Madelung, Springer-Verlag, N.Y., 1982.

4. C.A. Stolte, "Semiconductors and Semimetals", Vol.20, R.K. Willardson and A.C. Beer eds., Academic Press, N.Y., 1984, p. 152.

5. C.A. Stolte, pg. 119

6. J.B. Mullin, J. Cryst. Growth, 50 (1980) 625.

7. D.T.J. Hurle, J. Cryst. Growth, 50 (1980) 638.

8. R.L. Longini and R.F. Greene, Phys. Rev. 102 (1956) 992.

9. E. Scheil, Z. Metallk, 34 (1942) 70.

10. G.A. Baraff and M. Schlüter, Phys. Rev. Lett., 55(12) (1985) 1327.

11. G.M. Martin, Electronics Letters, 13 (1977) 191.

12. E.R. Weber and P. Omling, Adv. Sol. State Phys., 25 (1985) 623.

13. G.A. Baraff and M. Schlüter, Phys. Rev. B, 35(12) (1987) 6154.

14. G.A. Baraff and M. Schlüter, Phys. Rev. B, 33 (1986) 7346

15. D.V. Lang, J. Appl. Phys., 45 (1974) 3023.

16. J.M. Parsey, PhD Thesis, Department of Materials Science, MIT, Cambridge Mass., 1982.

17. M. Skowronski, J. Lagowski, and H.C. Gatos, J. Appl. Phys., 59 (1986) 2451.

18. G.M. Martin, Appl. Phys. Lett., 39 (1981) 747.

19. J.M. Parsey, Y. Nanishi, J. Lagowski, and H.C. Gatos, J. Electrochem. Soc., 129(2) (1982) 388.

20. E.M. Swiggard, S.H. Lee, and F.W. Von Batchelder, Conf. Ser. Inst. Phys. No. 45 (1979) 125.

21. J. Blanc and L.R. Weisberg, Nature, 192 (1961) 155.

22. R.N. Thomas, H.M. Hobgood, G.W. Eldridge, D.L. Barrett, T.T. Braggins, L.B. Ta, and S.K. Wang, "Semiconductors and Semimetals", Vol. 20, R.K. Willardson and A.C. Beer eds., Academic Press, N.Y., 1984, p. 6.

23. D.J. Stirland, M.R. Brozel, I. Grant, Appl. Phys. Lett., 46(11) (1985) 1066.

24. T. Kikuta, T. Katsumata , T. Obokata, K. Ishida, Proc. GaAs and Related Compounds, Biarritz 1984 (Conf. Ser. Inst. Phys. No. 74) p. 47-52.

25. D.E. Holmes, H. Kuwamoto, C.G. Kirkpatrick, and R.T. Chen, Proc. Semi-Insulating III-V Materials, Kahneetah 1984, Shiva, 1984, p. 204.

26. H. Okada, T. Katsumata, T. Obokata, and T. Fukuda, J. Cryst. Growth, 75 (1986) 319.

27. M. Duseaux, S. Martin, Proc. Semi-Insulating III-V Materials, Kahneeta 1984, Shiva, 1984, p. 118.

28. T. Shimada, K. Terashima, H. Nakajima, and T. Fukuda, Jpn. J. Appl. Phys., 23(1) (1984) L23.

29. T. Shimada, T. Obokata, and T. Fukuda, Jpn. J. Appl. Phys., 23(1) (1984) L441.

30. D.E. Holmes, R.T. Chen, K.R. Elliot, and C.G. Kirkpatrick, Appl. Phys. Lett., 40(1) (1982) 46.

31. D.C. Look, P.W. Yu, W.M. Theis, W. Ford, G. Mathur, J.R. Sizelove, D.H. Lee, and S.S. Li, Appl. Phys. Lett., 49(17) (1986) 1083.

32. T.S. Plaskett, J.M. Woodall, A.J. Segmuller, J. Electrochem. Soc., 118 (1971) 115.

33. C.E. Chang, W.R. Wilcox, J. Cryst. Growth, 21 (1974) 135.

34. C.N. Cochran and L.M. Foster, J. Electrochem. Soc., 109(2) (1962) 149.

35. E. Kubota and A. Katsui, J. Cryst. Growth 82 (1987) 573.

36. R. Ghez, S.E. Blum and M.B. Small, American Association for Crystal Growth Newsletter, 13(3) (1983) 5.

37. S.E. Blum and R.J. Chicotka, J. Electrochem. Soc., 120(4) (1973) 588.

38. H.H. Woodbury, J. Cryst. Growth, 35 (1976) 49.

39. W.A. Gault, E.M. Monberg and J.E. Clemans, J. Cryst. Growth., 74 (1986) 491.

40. C.G. Kirkpatrick, R.T. Chen, D.E. Holmes, P.M. Asbeck, K.R. Elliott, R.D. Fairman, and J.R. Oliver, "Semiconductors and Semimetals", Vol.20, R.K. Willardson and A.C. Beer eds., Academic Press, N.Y., 1984, p. 164.

41. J.M. Parsey Jr., and F.A. Thiel, J. Cryst. Growth, 73 (1985) 211.

42. S.M. Sze and J.C. Irvin, Solid State Electronics, 11 (1968) 599.

43. D.K. Ferry, "Gallium Arsenide Technology", Howard K. Sams and Co., Indianapolis Indiana, 1985.

44. S. Motojima, Y. Tamura, and K. Sugiyama, Thin Solid Films, 88 (1982) 269.

45. M. Sano, and M. Aoki, Thin Solid Films, 83 (1981) 247.

46. N. Yemenidjian and B.A. Lombos, J. Cryst. Growth, 56 (1982) 163.

47. P. Scherrer, Gottingen Nachrichten 2 (1918) 98.

48. G. Clark, "Encyclopedia of X-rays and Gamma Rays", Reinhold, 1963.

49. A. Zunger, A. Katzin, A. Halperin, Phys. Rev. B., 13 (12), (1976) 5560.

50. W. Walukiewicz, L. Lagowski, L. Jastrzebski, M. Lichtensteiger, and H.C. Gatos, J. Appl. Phys., 50(2), (1979) 899.

51. W.M. Theis, K.K. Bajaj, C.W. Litton, and W.G. Spitzer, Appl. Phys. Lett., 41 (1982) 70.

52. R.A. Morrow, J. Mater. Res.,2(5) (1987) 681.

53. D. Bliss, M.S. Thesis, University of California, Berkeley, 1988.

54. J.K. Kung and W.G. Spitzer, J. Appl. Phys., 45 (1974) 2254.

55. M.R. Brozel, K. Laithwaite, R.C. Newman, and B. Özbay, J. Cryst. Growth, 50 (1980) 619.

56. P.D. Greene, J. Cryst. Growth, 50 (1980) 612.

57. J. Leitner and F. Moravec, J. Cryst. Growth, 83 (1987) 376.

58. W.W. Theis and W.L. Spitzer, J. Appl. Phys., 56 (1984) 890

59. M.R. Brozel, J.B. Clegg, and R.C. Newman, J. Phys. D, 11 (1978) 1331.

60. J. Lagowski, H.C. Gatos, J.M. Parsey, K. Wada, M. Kaminska, and W. Walukiewicz, Appl. Phys. Lett., 40(4) (1982) 342.

61. J.R. Knight, Nature, 190 (1961) 1001.

62. H. Schafer, "Chemical Transport Reactions", Academic Press, N.Y. (1964).

63. C.N. Cochran and L.M. Foster, J. Electrochem. Soc., 109 (1962) 144.

LAWRENCE BERKELEY LABORATORY
TECHNICAL INFORMATION DEPARTMENT
UNIVERSITY OF CALIFORNIA
BERKELEY, CALIFORNIA 94720